



**Poly (Ethylene Oxide)/Graphene Oxide Polymer Nanocomposite Electrolyte for  
Lithium Ion Batteries**

A Thesis

Presented to

the Faculty of the Department of Mechanical Engineering  
University of Houston

In Partial Fulfillment

of the Requirements for the Degree

Master of Science

in Mechanical Engineering

by

Mengying Yuan

August 2013



## Acknowledgements

Although only my name is on the cover of this thesis, this thesis would not have been accomplished without the contribution of a great number of people. In the beginning, I must give my great thanks to my parents, who gave me life and supported me all the time. With their support, I have the opportunity to further my education here which will benefit my whole life.

Now I would like to express my deep and sincere gratitude to my advisor, Dr. Haleh Ardebili, for accepting me as her Master's student. I am grateful that you have supported me throughout this thesis and treated me well and respectfully. Thank you for your encouragement, and for believing in me. I've learned so much about science, and so much about life. Without your help, time and guidance, my experience over these years would not have been so amazing and productive. Thank you for this opportunity!

I would like to acknowledge my financial support from TcSUH, the Texas Center for Superconductivity at the University of Houston. I would like to thank Dr. Yao one of my thesis committee members for all the lively discussions and constructive feedback about my research. I would also like to acknowledge Dr. Ryou for his participation as a committee member and his dedication and invaluable comments about this thesis.

I would like to give special thanks to Jeremy Erdman for his help with the Fourier Transform Infrared (FTIR) testing and analysis. Also I could not finish this work without the help of Qin Li; as a senior Ph. D student of Dr. Ardebili, he gave me a lot of help. I also acknowledge Sridharreddy Appanapalli and Eric Wood for their help with the electrochemical experiments. Lastly, I want to thank all the other members in our lab,

Mejdi Kammoun and Taylor Dizon. Without their support, I would never have finished this work successfully.

**Poly (Ethylene Oxide)/Graphene Oxide Polymer Nanocomposite Electrolyte for  
Lithium Ion Batteries**

An Abstract  
of a  
Thesis  
Presented to  
the Faculty of the Department of Mechanical Engineering  
University of Houston

In Partial Fulfillment  
of the Requirements for the Degree  
Master of Science  
in Mechanical Engineering

by  
Mengying Yuan

August 2013

## **Abstract**

Solid polymer electrolytes (SPEs) can resolve the safety problems associated with the traditional liquid electrolytes while offering mechanical stability and thin film manufacturability. The main issue with SPEs is the lower ionic conductivity at room temperature compared to that of liquid electrolytes. Nanosized ceramic powders are known to enhance the ionic conductivity as well as the mechanical stability of solid polymer electrolytes.

In this study, graphene oxide (GO) nanosheets were used as nanosized fillers in polyethylene oxide (PEO) electrolyte. We demonstrated that about an order of magnitude improvement in lithium-ion conductivity, as high as  $10^{-4}$  S/cm at room temperature, was achieved with GO fillers. We used thermal analysis, impedance spectroscopy, fourier transform infrared, and morphology analysis to investigate the GO/PEO films. A significant improvement in the tensile strength of the polymer electrolyte was observed with only 1 wt % GO fillers while the % elongation remains uncompromised.

# Table of Contents

Acknowledgements.....	iv
Abstract.....	vii
Table of Contents.....	viii
List of Figures.....	x
List of Tables.....	xiii
Chapter 1 Solid Polymer Electrolytes for Lithium-ion Batteries .....	1
1.1 Introduction of Lithium-ion Battery .....	1
1.2 Overview of Solid Polymer Electrolytes for Lithium-ion Batteries .....	3
1.3 Ion Conductivity Mechanism in Solid Polymer Electrolytes .....	5
1.4 Ion Conductivity Enhancement at Ambient Temperature .....	8
1.4.1 The Introduction of Gel-Type Polymer Electrolyte.....	8
1.4.2 Polymer Nanocomposite Electrolytes for Lithium-ion Batteries.....	9
Chapter 2 Experiments .....	16
2.1 Materials .....	16
2.2 Equipment.....	17
2.3 Fabrication of PEO/LiClO <sub>4</sub> Nanocomposite Solid Polymer Electrolytes.....	20
2.3.1 Preparation of The Filler Free 100,000 Molecular Weight PEO Films.....	20
2.3.2 Preparation of GO Based Solid Polymer Nanocomposite Electrolyte.....	21



2.4	Characterization .....	23
2.4.1	Complex Impedance Spectroscopy .....	23
2.4.2	Dynamic Mechanical Analysis .....	27
2.4.3	Differential Scanning Calorimetry .....	29
2.4.4	Scanning Electron Microscope .....	30
2.4.5	Fourier Transform Infrared Spectroscopy .....	31
Chapter 3	Results and Discussions .....	32
3.1	Ion Conductivity .....	32
3.2	Mechanical Property and Application (Stress/Strain Rate) .....	37
3.3	Thermal Analysis .....	40
3.4	Morphology .....	44
3.5	Fourier Transform Infrared Spectroscopy .....	48
Chapter 4	Conclusions and Summary .....	50
4.1	Conclusions .....	50
4.2	Summary .....	51
References	.....	52

## List of Figures

Figure 1.1 Comparison of different battery technologies in terms of volumetric and gravimetric energy densities. ....	1
Figure 1.2 The lithium-ion battery mechanism .....	2
Figure 1.3 Schematics of solid polymer electrolyte based lithium-ion battery .....	4
Figure 1.4 Cation motion in a polymer electrolyte assisted by polymer chains .....	7
Figure 1.5 Link between electrolyte composition, properties, and battery performance .	10
Figure 1.6 Schematic representation of polymer chain and inert filler of (a) nanosize (b) micron size in composite polymer electrolytes .....	11
Figure 1.7 Arrhenius plots of the conductivity of ceramic-free PEO–LiClO <sub>4</sub> and of polymer nanocomposite .....	12
Figure 1.8 Oxidation of pure graphite powder to graphite oxide .....	13
Figure 1.9 Graphene oxide structure.....	14
Figure 1.10 The schematic of the PEO/GO membrane .....	15
Figure 2.1 The SEM image of graphene oxide from Graphene Supermarket .....	17
Figure 2.2 Glovebox system. ....	19
Figure 2.3 Magnetic stirring plate.....	19
Figure 2.4 Vacuum ovens. ....	19
Figure 2.5 Fourier transform infrared spectroscopy. ....	20
Figure 2.6 Pure PEO/Li membrane.....	21
Figure 2.7 PEO/GO solution before and after stirring.....	22
Figure 2.8 GO based PEO/Li membranes.....	22
Figure 2.9 Equivalent circuit model.....	23

Figure 2.10 “Sandwich” test sample used in ion conductivity measurement. ....	24
Figure 2.11 FRA impedance potentiostatic procedures. ....	25
Figure 2.12 Frequency set. ....	26
Figure 2.13 A standard nyquist plot. ....	26
Figure 2.14 Stress/strain measurements. ....	27
Figure 2.15 Strain rate procedures. ....	28
Figure 2.16 The elongation of the film during the DMA tensile test. ....	28
Figure 2.17 The DSC heat/cool/heat procedure. ....	30
Figure 2.18 Polymer nanocomposite electrolyte samples. ....	31
Figure 3.1 Nyquist plot of GO based polymer nanocomposite electrolytes. ....	33
Figure 3.2 Relationship between ionic conductivity and filler concentration and relationship between ionic conductivity improvement and filler concentration. ....	34
Figure 3.3 GO fillers (a) aligned with diffusion (b) blocking diffusion and (c) trapping ions. ....	36
Figure 3.4 Comparison of Stress/Strain curves of electrolyte films. ....	38
Figure 3.5 A Comparison of the tensile Stress-Strain curves measured for the PEO-Li based electrolyte films [37]. ....	39
Figure 3.6 DSC traces as a function of graphene oxide concentration. ....	41
Figure 3.7 The relationship between glass transition temperature and GO concentration. .....	41
Figure 3.8 PEO crystalline fraction as a function of GO concentration for all samples...	42
Figure 3.9 SEM picture of pure PEO-Li polymer electrolyte. ....	45

Figure 3.10 SEM image of (a) Filler Free polymer electrolyte (b) 0.5 wt. % GO (c)	
1wt. % GO (d) 5wt. % GO/PEO-Li polymer electrolyte.....	46
Figure 3.11 SEM picture of 1 wt. % GO/PEO-Li polymer electrolyte.....	47
Figure 3.12 SEM image of cross sectional morphology of 1 wt. % GO/PEO-Li polymer	
electrolyte.....	47
Figure 3.13 FTIR spectra of pure GO, pure PEO, filler free, 0.5% GO, 1% GO and 3%	
GO polymer electrolytes. ....	49
Figure 3.14 Li salt dissociation fractions of pure and filled polymer species from FTIR.	49

## **List of Tables**

Table 1.1 The physical and electrochemical properties of various electrolytes for lithium-ion battery .....	8
Table 2.1 Materials used in experiment.....	16
Table 2.2 Equipment used in experiments .....	17
Table 2.2 Equipment used in experiments, (continued) .....	18
Table 3.1 Complex impedance spectroscopy results .....	33
Table 3.2 Ion conductivity reported from other fillers at room temperature .....	34
Table 3.2 Ion conductivity reported from other fillers at room temperature, (continued) .....	35
Table 3.3 DSC thermal properties of solid polymer electrolyte in our study .....	43

# Chapter 1 Solid Polymer Electrolytes for Lithium-ion Batteries

## 1.1 Introduction of Lithium-ion Battery

Lithium-ion batteries have received significant attention in recent years. The energy density of lithium-ion battery far exceeds that of other batteries such as nickel-cadmium, nickel-metal-hydride, or lead-acid (Fig. 1.1). In other words, more electrochemical energy can be stored in a lithium-ion battery per unit volume or unit mass than many other technologies [1]. The lithium element is an outstanding candidate material for batteries due to its lowest standard potential and electrochemical equivalence. It is only inferior on a volumetric energy basis to aluminum and magnesium. However, aluminum has not been used successfully as an anode material due to its poor electrochemical behavior [2]. Furthermore, lithium is preferred to other alkali metals due to better mechanical stability and lower reactivity [3].

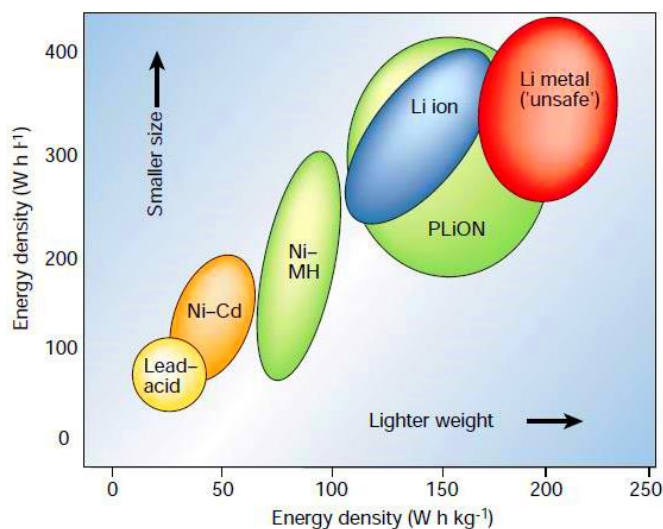


Figure 1.1 Comparison of different battery technologies in terms of volumetric and gravimetric energy densities [1].

A typical lithium-ion battery consists of a cathode, an anode and an electrolyte. The electrolyte must be both an ion conducting and electrically insulating material. In the case of liquid electrolytes, a separator is needed for the physical separation of the electrodes. In a battery's electrochemical cell, the main paths of electrons and ions must be separated from each other. The ions move through the electrolyte and the electrons leave the battery through the external circuit leading to a usable electrical current (Fig. 1.2). After a while, the supply of the ions from the negative pole is used up and the battery needs to be recharged. The recharging takes place in the same way, but now reversed and the ions move from the positive to the negative pole [1].

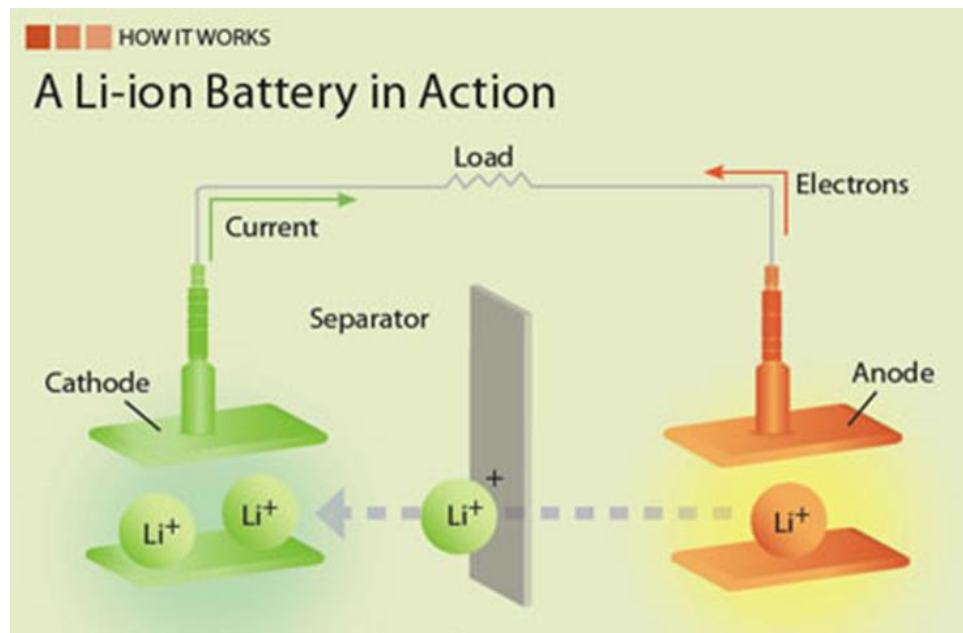


Figure 1.2 The lithium-ion battery mechanism [4].

The first set of lithium-based batteries used pure lithium metal as the anode; however, these batteries suffered from the decomposition of the organic liquid electrolyte and lithium dendrite growth through the electrolyte. For these types of batteries, it is highly

imperative to replace the liquid electrolyte with a solid or viscous gel polymer electrolyte [5]. Even for the LIBs without lithium metal anodes, the dendrite growth and safety issues associated with liquid electrolytes can persist but with less severity. Furthermore, a battery based on a solid polymer electrolyte generally does not require a heavy case, because it is nontoxic, nonflammable, and stable. All these advantages combined with the mechanical properties of a polymer, make the solid and gel polymer electrolytes highly attractive and would permit the design of a mechanically flexible battery of varying shapes and sizes [6].

## 1.2 Overview of Solid Polymer Electrolytes for Lithium-ion Batteries

As a medium for transporting ions during charge and discharge cycles of the battery, the solid polymer electrolyte also acts as a separator between the cathode and the anode (Fig. 1.3). The electrolyte type and electrode/electrolyte interface characteristics, however, are also crucial factors affecting the battery power, cost, life, and safety. The battery's complete electrochemical reactions require the electrons and lithium ions be fully transported from one electrode to another. The limited mobility (or ionic conductivity) of the  $\text{Li}^+$  cations through the solid electrolyte interface and bulk electrolyte is the most important contributor to the limited battery power [7]. Most rechargeable lithium-ion batteries contain a flammable organic liquid electrolyte. These batteries have a tendency to leak and in the worst situation, the evaporation of solvent may lead to fire hazards.



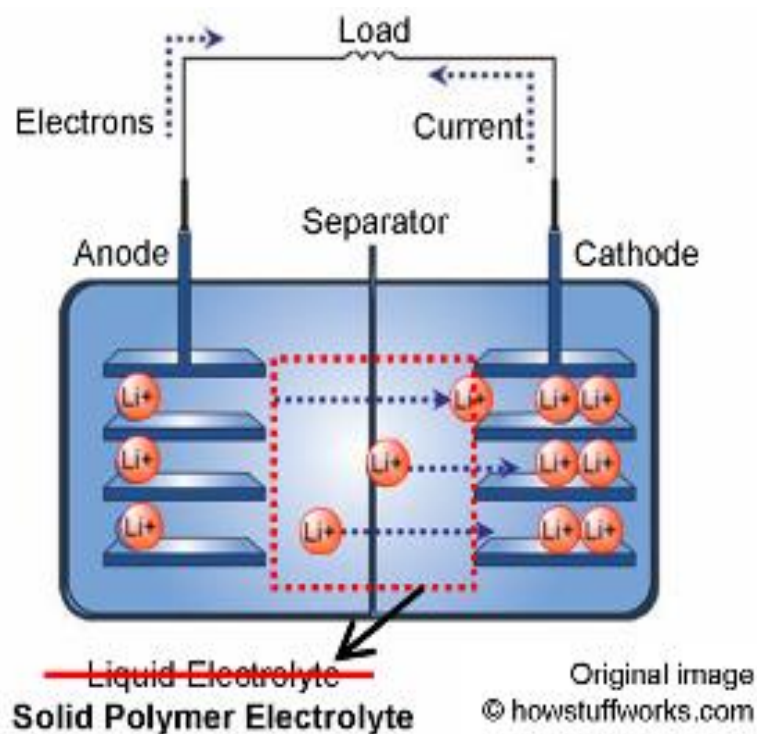


Figure 1.3 Schematics of solid polymer electrolyte based lithium-ion battery.

Recently, solid polymer electrolyte have attracted much attention because they offer safety, stability and processability [8]. After the discovery of ionic conductivity in alkali metal salt complexes of PEO (polyethylene oxide) in 1973 [9], researchers concentrated on solid polymer electrolytes properties including the electrochemical stability, ion conductivity, chemical and electrochemical compatibility, mechanical properties and thermal stability. Polymer electrolytes were first proposed for batteries in 1978 [10]. Besides the safety and environmental friendliness, the PEO electrolyte exhibits several advantages on the molecular level. It has a specific spacing between the oxygen groups leading to a five-membered ring type structure which is desirable for cation solvation at the oxygen sites. For example, both  $-(\text{CH}_2\text{CH}_2\text{CH}_2)_n-$  and  $-(\text{CH}_2)_n-$  are much

weaker solvents. Therefore, the SPEs and commonly used PEO systems can become key electrolyte materials for the next generation of lithium-ion batteries.

Unfortunately, a key challenge is the lower ion conductivity of the solid polymer electrolyte especially at room temperature compared to conventional liquid electrolytes. Nanoparticles have been shown to improve ion conductivity of polymer electrolytes up to 3 orders of magnitude [11].

### 1.3 Ion Conductivity Mechanism in Solid Polymer Electrolytes

In order to establish how nanoparticles improve the ion conductivity in SPEs, we must first understand how ions move through the electrolyte in an unfilled system. M. B. Armand first proposed the application of a dry polymer electrolyte to a battery [12] after the discovery of ionic conduction in the polyethylene oxide (PEO) by P. V. Wright [13]. The dry polymer electrolyte consisted of a polymer host and alkali metal salts. The polymer hosts have polar groups (repeated functional groups) that can interact with cations, such as etheric oxygen in oxy-ethylene or oxy-propylene unit. High solubility of the salt, easy ion dissociation, and easy ion diffusion are required functions for a polymer host. The ion dissociation unit such as ethylene-oxide and ethylene-imine in polymer structures accelerate the dissociation of electrolyte salts into ions.

At first, most people thought that the crystalline domain of a polymer was mainly responsible for the ion transport with the primary mechanism postulated as the ions move along the PEO helices. However, it was soon established that it is mainly the amorphous phase that gives rise to ion transport [14] with the exception of some special crystalline Li complexed polymer compounds. Lithium ions generally tend to move through the amorphous domains of the polymer by making and breaking complexes with the help of

ether oxygen atoms, and the mobility of Li<sup>+</sup> is facilitated by the polymer's segmental relaxation. Since ion and polymer mobility are coupled, the mission to improve conductivity have mainly concentrated on increasing polymer mobility in the amorphous phase [6]. The ionic conductivity can be expressed by

$$\sigma = ne\mu, \quad (1)$$

$n$ : the effective number of mobile ions

$e$ : the elementary electric charge

$\mu$ : the ion mobility.

Since the fraction of “free” ions is an important parameter, a high degree of salt dissociation in the polymer can lead to improved conductivity [5].

Molecular dynamics simulations suggest that the Li<sup>+</sup> ions are complexed to PEO matrix through approximately five ether oxygens of a PEO chain, and thus the mobility of the cations is dropped considerably by this complexation [15]. Consequently, the mobility of the Li cations is related to the motions of the complexing segments of the PEO chain. Thus, assisted by the segmental motion of the PEO matrix, the cation transport is described as the motion of the Li<sup>+</sup> between complexation sites. As a result of the motion of polymer chains, cations are able to “hop” between the coordination sites among the neighboring chains, which is called interchain and intrachain hopping.

Ion transportation facilitated by the polymer host is greatly affected by not only the polymer micro-relaxation which determines the dynamic property of the polymer, but also the segmental motion of the polymer chain. The polymer segmental motions are thought to promote ion mobility by making and breaking the co-ordination bonds between cation

and polymer and also providing free volume where the ion can diffuse through as shown in Fig. 1.4.

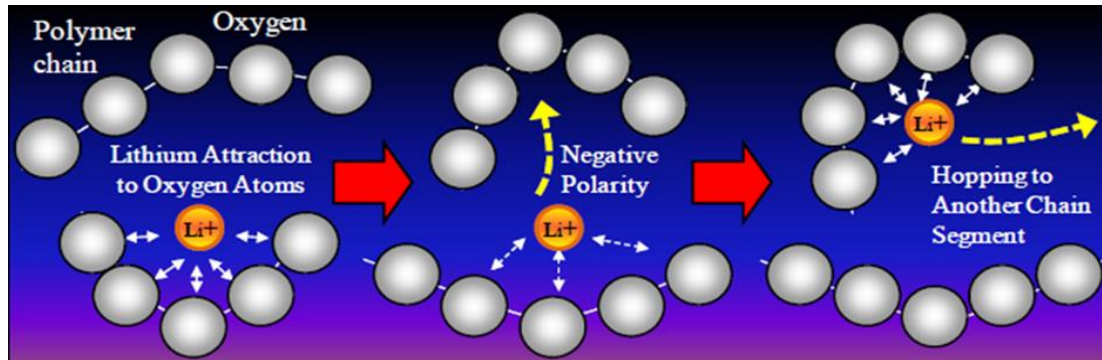


Figure 1.4 Cation motion in a polymer electrolyte assisted by polymer chains [16].

Temperature plays an important role in the ion transport phenomenon. Since the relaxation of polymer and its segmental motion greatly depend on temperature, the ionic conductivity of the polymer electrolyte is also highly temperature dependent [17]. As the temperature is increased, the local nano and micron-sized voids may be produced by material expansion, allowing the polymer segments, ionic species or solvated molecules to move through this free volume. A distribution function for the size of voids in the given material can be derived, and the probability of this distribution can be maximized [18]. Amorphous and semi-crystalline solid polymer electrolytes therefore require local relaxation and segmental motion of the polymer (PEO) chains to allow ion ( $\text{Li}^+$ ) transport. This condition can be accelerated when the polymer is above the crystallization and melting temperatures, that is, above  $60^\circ\text{C}$  in the case of PEO [19].

## 1.4 Ion Conductivity Enhancement at Ambient Temperature

Generally, the polymer electrolytes in lithium-ion batteries are classified into two types of electrolytes: one is a dry-type electrolyte composed of polymer matrix and the electrolyte salt; the other is a gel-type electrolyte in which polar solvent is added as plasticizer to an appropriate polymer matrix [17].

Table 1.1 The physical and electrochemical properties of various electrolytes for lithium-ion battery [20].

<b>Property</b>	<b>Organic carbonated-based electrolytes</b>	<b>Ionic liquid-based electrolytes</b>	<b>Solid polymer electrolytes (SPE)</b>	<b>Polymer gel electrolytes(GPE)</b>
Mechanical	low flexibility and stability	low flexibility and stability	high flexibility and stability	moderate flexibility and stability
Electrochemical and chemical stability	moderate	low or moderate	high	moderate
Thermal stability	low	high	high	moderate
Conductivity	high	high or moderate	very low	moderate
Lithium selective transference	high	low	high	high

### 1.4.1 The Introduction of Gel-Type Polymer Electrolyte

The purpose of plasticizing the polymer electrolyte matrix is to reduce the local viscosity and thereby facilitating the mobile ion ( $\text{Li}^+$ ) to move faster within the medium which in turn enhances the mobility and hence the conductivity. An improvement in the conductivity of several orders of magnitude can be obtained with the addition of liquid plasticizers such as propylene carbonate. When the amount of plasticizer used is high (as high as 70%) the result is a noticeably diminished chemical and mechanical stability

compared to the solvent free solid systems. These electrolyte systems with high percentage of plasticizers are more appropriately described as “gel” polymer electrolytes. The loss of mechanical stability is largely the result of the melting of crystalline phase. However, it is anticipated that these systems are inherently more desirable than liquid-based electrolyte systems in terms of safety, due to the fact that the solvents are contained in the polymeric structure with the associated interacting forces [21].

The class of polymer electrolytes called “gel” electrolytes typically contains trapped liquid solutions of lithium salts in aprotic organic solvents within a solid polymer matrix such as polyacrylonitrile. Conductivities of these polymers can be much higher than dry solid polymers and the partially plasticized polymers. However, these plasticized and gel electrolytes have a limited chemical stability and can be more reactive with lithium than the solid polymers.

#### **1.4.2 Polymer Nanocomposite Electrolytes for Lithium-ion Batteries**

The goal in this study is to obtain a new class of solid polymer electrolytes having unique properties such as low thermal conductivity and high ion conductivity (both promoted by the high aspect ratio of the dispersed fillers) and improved mechanical stability induced by the network of the dispersed fillers (Fig. 1.5). Polymers have been reinforced for many years with various inorganic fillers of macro- or micrometer dimensions and as a result newly formed materials carried the filler properties [22]. This may have caused many problems during the production such as undesired stiffening and toughness. Therefore, composites and nanometer-size materials were integrated to change the nature of the reinforcement [23]. In early 1990s, scientists started to use very fine materials of nanometer sizes. However, many of the fine particles did not lead to good

reinforcement. They tended to agglomerate rather than disperse in the solution. The idea of new effective material is having well dispersed fillers to form a strong bond with the polymer and then tie the properties of the new material to the interface [24].

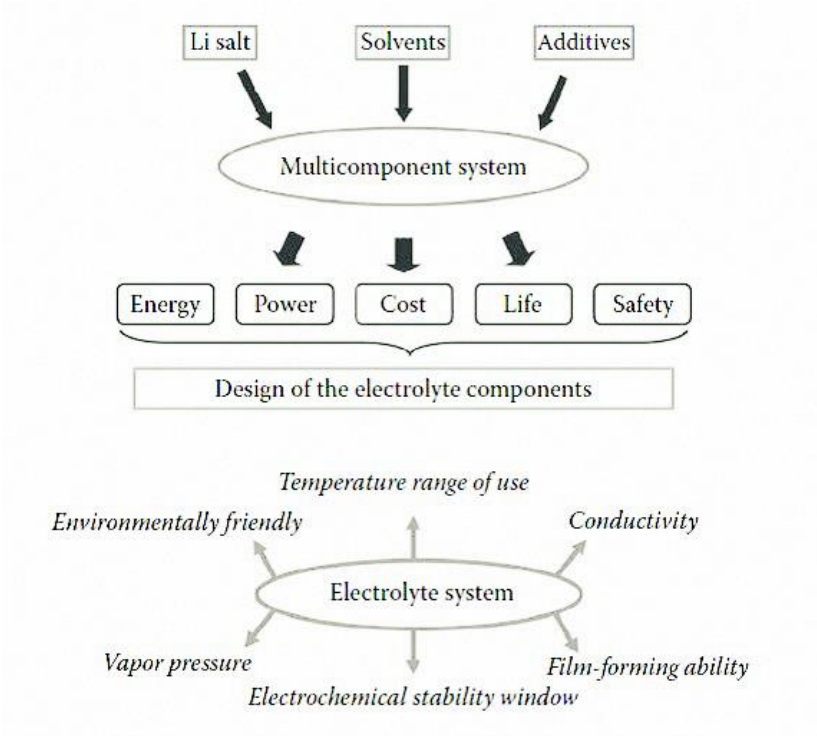


Figure 1.5 Link between electrolyte composition, properties, and battery performance [7].

#### 1.4.2.1 Traditional Ceramic Powders as Fillers for SPE

In recent years, many researchers have promoted the development of composite polymer electrolytes by introducing fillers such as  $\text{Al}_2\text{O}_3$ ,  $\text{SiO}_2$ ,  $\gamma\text{-LiAlO}_2$ ,  $\text{TiO}_2$  [20] resulting in improved mechanical properties, enhanced ionic conductivity, and better interfacial stability between lithium and the polymer electrolyte. Compared to pure polymer electrolytes, the main advantages of ceramic filled polymers are:

- higher conductivities;
- increased transference number;

- better thermodynamic stability towards lithium and other alkali metals.

The ceramic particles, depending upon the volume fraction, tend to minimize the area of lithium electrode exposed to polymers containing O, OH<sup>-</sup> species and thus reduce the electrode/electrolyte interface passivation process. It is also foreseeable that smaller size particles for a similar volume fraction of the ceramic phase would impart an improved performance as compared to larger size particles because they can cover more surface area. The formation of an insulating layer of ceramic particles at the electrode surface is probable at higher volume fraction of a passive ceramic phase. The insulating layer can impede electrode reactions. When the passive and relatively inert ceramic phase is introduced into the polymer matrix this can occur successfully [25]. Schematic diagrams of the lithium-composite electrolyte interfaces are shown in Fig. 1. 6 (a) and (b).

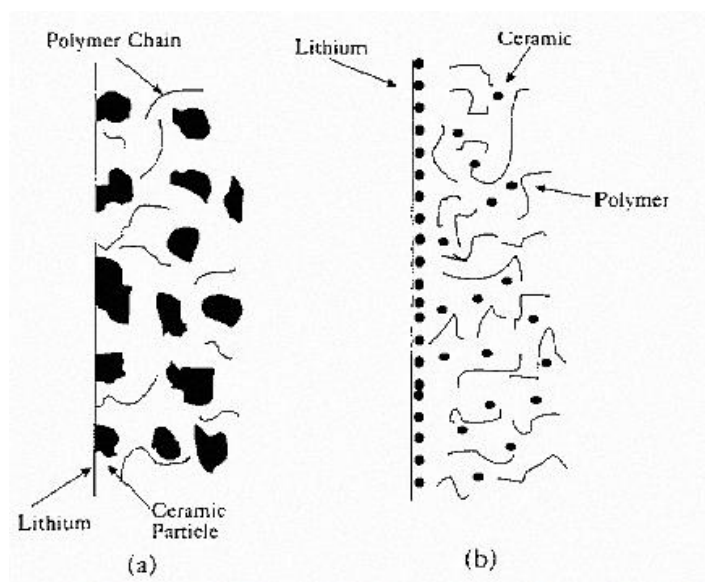


Figure 1.6 Schematic representation of polymer chain and inert filler of (a) nanosize (b) micron size in composite polymer electrolytes [25].

An intriguing class of new polymer nanocomposite materials is composed of layered silicates intercalated by polymer chains. They combine the two concepts,



composites and nanometer-size materials. The reinforcement effect of the nanoparticles is usually based on chemical connections, which forms a network between nanoparticles and the polymer matrix. For both the conducting and inert ceramics, conductivity enhancement is observed as a result of adding the ceramic powder and is attributed to an increase in the volume fraction of the amorphous phase. More detailed studies of nanocomposite fillers revealed that grain size, phase boundary resistances, phase composition and  $T_g$  are all contributing factors to the conductivity of the nanocomposite polymer electrolytes and make the analysis of the ion transport very complex. Figure 1.7 shows the relationship of ion conductivity and filler type in different temperatures.

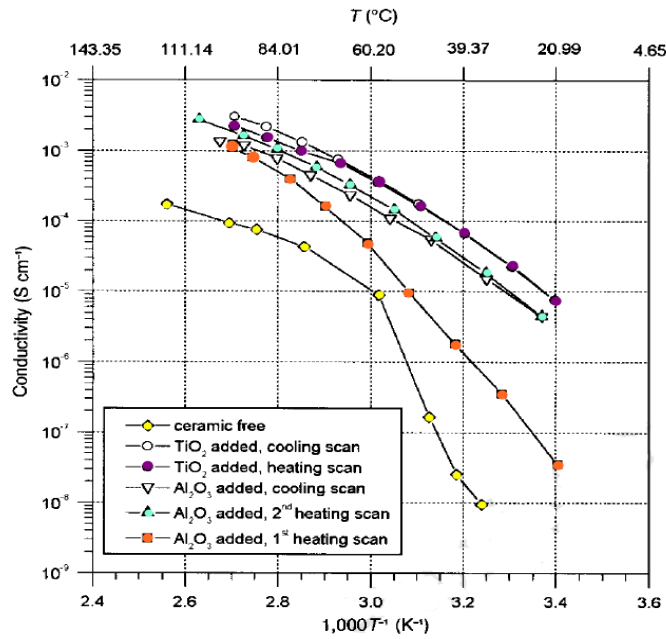


Figure 1.7 Arrhenius plots of the conductivity of ceramic-free PEO-LiClO<sub>4</sub> and of polymer nanocomposite [19].

There is an obvious break around 60°C, which reflects the melting temperature of the PEO and the transition from solid semi-crystalline state of PEO to liquid amorphous state. This was accompanied by an increase in ionic conductivity. The trend of the curve is

reproduced in the following cooling scan; this confirms, when brought back to low temperature, as the PEO–LiClO<sub>4</sub> electrolyte solidifies and partially recrystallizes, the conductivity decays [19].

#### 1.4.2.2 PEO/GO Nanocomposite Membrane as SPE

Two-dimensional nanosheet of graphene oxide (GO) can be a promising filler material for polymer electrolyte. Researchers have postulated that the hydration of GO can incorporate the water molecule between GO sheets which presumably form hydrogen bonds [26].

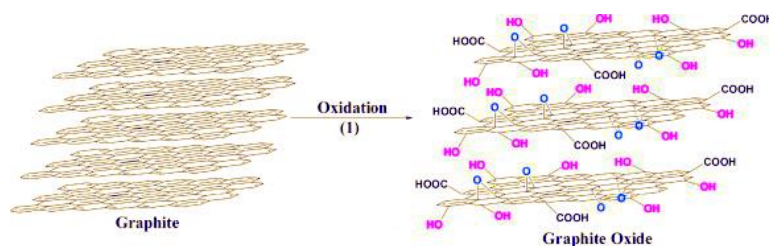


Figure 1.8 Oxidation of pure graphite powder to graphite oxide.

GO and hydrophilic polymers are highly compatible for the formation of composite membranes in which the H<sup>+</sup> will be released from the –COOH groups on the sheets of GO in the polymer matrix (Fig. 1.8). Expandable graphite has been reported to easily introduce more functional groups into its galleries than natural graphite by treatment with sulphuric acid and these groups have been experimentally observed, including carbonyl (CO), Hydroxyl (–OH), carboxyl (–COOH), phenol groups, and oxygen epoxide groups (bridging oxygen atoms).

The polar oxygen functional groups of GO render it hydrophilic; GO can be exfoliated in many solvents, and disperses particularly well in water, breaking up into

macroscopic flakes, which are mostly one layer thick. Scanning tunneling microscopy shows oxygen atoms on GO are arranged in a rectangular pattern with a lattice constant of  $0.27 \text{ nm} \times 0.41 \text{ nm}$ [27]. Furthermore, pure GO itself is an electronic insulator [17, 18].

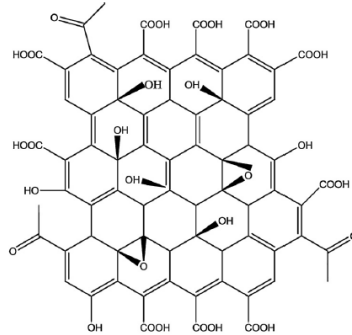


Figure 1.9 Graphene oxide structure.

The GO exhibits dramatically improved properties compared with either their pure inorganic constituent or polymer components. Since inorganic constituents are in the nanoscale dimensions and have an enormous surface area with respect to volume, most of the polymer is present near the interface. This high specific surface area can change the nature of the reinforcement.

Therefore, GO is a potentially effective filler for solid polymer electrolytes for lithium-ion battery. Figure. 1.10 shows a schematic of PEO/GO solid polymer electrolyte [28].

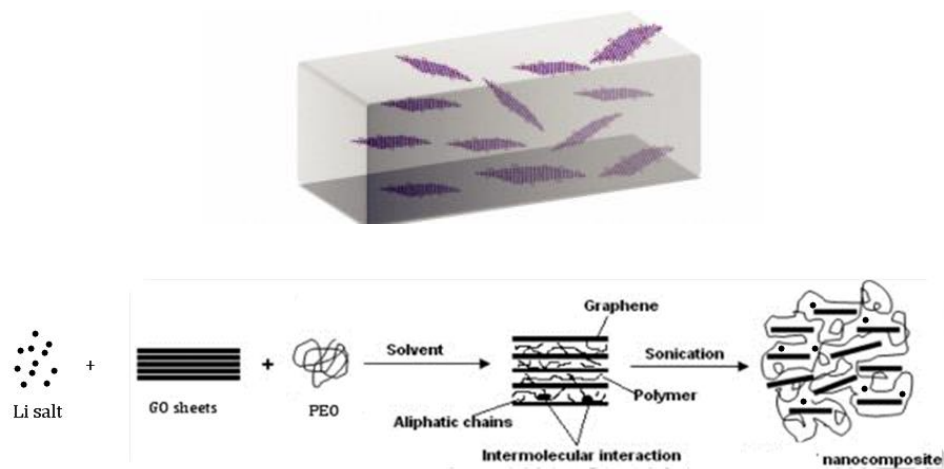


Figure 1.10 The schematic of the PEO/GO membrane [28].

## Chapter 2 Experiments

### 2.1 Materials

The molecular formula, weight, and structure, chemical name, concentration and source of materials used in the experiments in this thesis are listed in Table 2.1 PEO is used as the main polymer matrix, the lithium salt used is  $\text{LiClO}_4$ , acetonitrile is the solvent, and graphene oxide (GO) is explored as the nanofiller.

Table 2.1 Materials used in experiment.

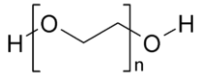
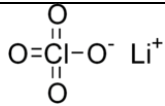
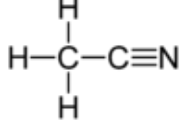
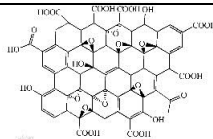
Name	Molecular Formula	Molecular Structure	Molecular Weight	Concentration /Ratio	Source
Polyoxyethylene	$\text{H}-(\text{O}-\text{CH}_2-\text{CH}_2)_n-\text{OH}$		100,000	N/A	Sigma-Aldrich
Lithium Perchlorate	$\text{LiClO}_4$		106.4	16:1(Li : O)	Sigma-Aldrich
Acetonitrile	$\text{C}_2\text{H}_3\text{N}$		41.05	N/A	Sigma-Aldrich
Graphene Oxide	N/A		N/A	N/A	Graphene Supermaket

Figure 2.1 shows the scanning electron microscopy (SEM) image of the GO used in the experiments. It has improved dispersibility in various solvents. Graphene oxide layer sizes are about 0.5-5 microns in length and width and about  $1.1 \pm 0.2$  nm in thickness.

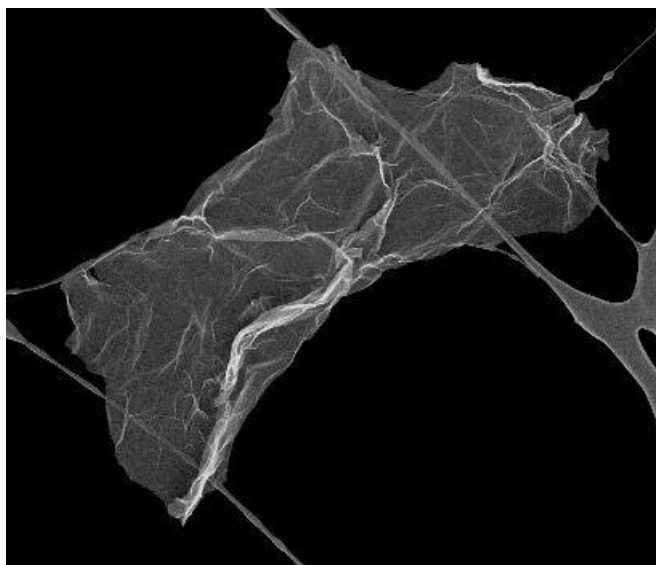


Figure 2.1 The SEM image of graphene oxide from Graphene Supermarket.

## 2.2 Equipment

The name, type, function and source of equipments used in the experiments are listed in Table. 2.2.

Table 2.2 Equipment used in experiments.

Name	Type	Function	Source
Magnetic Stirrer	RT 15 power	Mixing and stirring	IKAMAG®
Analytical Balance	PA 200 C	Weighting	Intell-Lab™
Vac Glovebox Systems	Dual Port-Omni-Lab	Battery Assembly and Dry Storage	Vacuum Atmospheres Company
Vacuum Oven	N/A	Dry	SHELAB
AutoLab	N Series	Ionic Conductivity	Metrohm

Table 2.3 Equipment used in experiments, (continued).

Name	Type	Function	Source
Dynamic Mechanical Analysis	Q 800	Mechanical Analysis	TA Instruments
Differential Scanning Calorimetry	Q 2000	Thermal Analysis	TA Instruments
Scanning Electron Microscope	N/A	Morphology Analysis	N/A
Fourier Transform Infrared	Cary 630	Dissociation Analysis	Agilent Technologies

Figure 2.2, shows the dry glove box used to store the initial constituent materials and the final products. The glove box consists of two ante chambers (large and small) which enable the transfer of objects of various sizes inside and outside the glove box. The solution was stirred on a magnetic stirring plate shown in Figure 2.3. The whole process of solution preparation should be done under stirring. The membranes were dried in the vacuum ovens shown in Figure 2.4. During the drying process, the vacuum should run continuously to ensure that the membranes are dry enough.



Figure 2.2 Glovebox system.



Figure 2.3 Magnetic stirring plate.



Figure 2.4 Vacuum ovens.





Figure 2.5 Fourier transform infrared spectroscopy.

## 2.3 Fabrication of PEO/LiClO<sub>4</sub> Nanocomposite Solid Polymer Electrolytes

The polymer electrolyte films were prepared by the dissolution of calculated amounts of dried lithium salt and PEO powder in acetonitrile solvent and the removal of the solvent under vacuum. A detailed description of the fabrication process is presented in this section.

### 2.3.1 Preparation of the Filler Free 100,000 Molecular Weight PEO Films

The Li salt powder (0.3 g) was first completely dissolved in the acetonitrile in a round-bottom bottle. The PEO powder (2 g) was then dissolved in 30 mL acetonitrile in another bottle. Both of them were under stirring for 6 hours. Then, they were mixed together and stirred for another 3 hours to obtain the PEO/Li salt solution. The mixed solution was poured into a prepared non-stick Teflon petri dish and was subsequently, placed inside the vacuum oven at 50 °C for 24 h until the membrane was sufficiently dry.



Figure 2.6 Pure PEO/Li membrane.

### 2.3.2 Preparation of GO Based Solid Polymer Nanocomposite Electrolyte

The first two steps mentioned in the previous section for the pure polymer film, was repeated for the GO filled films except that they were prepared for 5 different GO contents. Graphene oxide powder with contents of 0.5%, 1%, 3%, 5% 8% were added to bottles and initially stirred for 6 hours. Then, the bottles with PEO, GO and Li salt were mixed together and stirred for another 3 hours to obtain the PEO/GO/Li salt solution. The mixed solution was sonicated for 25 min and the PEO/GO solutions were poured into different Teflon petri dishes and kept in the oven at 50 °C for 24 h until the membranes were dry.



Figure 2.7 PEO/GO solution before and after stirring.

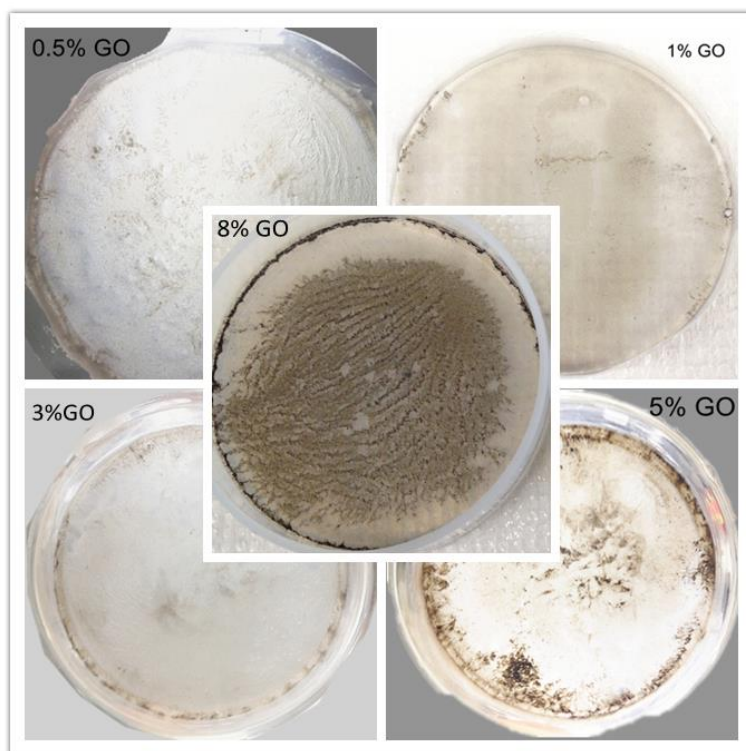


Figure 2.8 GO based PEO/Li membranes.

It can be observed from Figure 2.8 that the graphene oxide fillers aggregate during the drying process due to their high aspect ratio and high surface energy. The aggregation is more significant with higher filler contents. In 5% GO film, we can clearly see clusters of the graphene oxide. In case of 8% GO, the film is full of clusters and the graphene oxide is barely dispersed in the PEO matrix.

## 2.4 Characterization

### 2.4.1 Complex Impedance Spectroscopy

PGSTAT/Metrohm Autolab was used to measure the ionic conductivity at room temperature. The complex impedance spectroscopy was obtained by FRA measurement potentiostatic model. Figure 2.9 shows the equivalent circuit model used. It can describe the electrolyte processes when both kinetics and diffusion are important. The samples were placed between two stainless steel electrodes shown in the Figure 2.10.

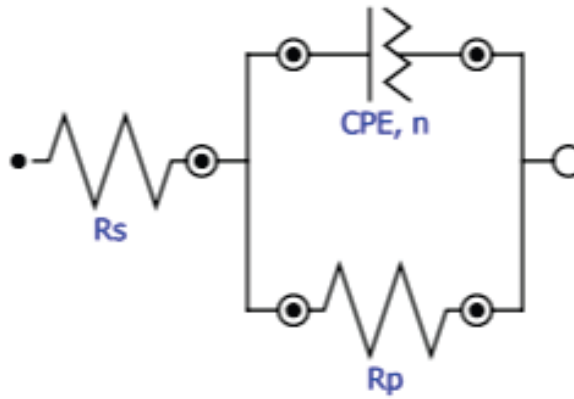


Figure 2.9 Equivalent circuit model.

This circuit includes the following items:

- $R_s$  (Ohm) – used to simulate the value of the uncompensated resistance

- $R_p$  (Ohm) – used to simulate the polarization resistance (also referred to as the charge transfer resistance)
- CPE – the value of the argument of the constant phase element (also referred to as a Q element)
- $n$  – the value of the exponent of the constant phase element



Figure 2.10 “Sandwich” test sample used in ion conductivity measurement.

The scan frequency is from 1 to 1,000 kHz. The value of the applied amplitude is 0.02 V (Fig. 2.11, 2.12).

FRA impedance potentiostatic		
Remarks	FRA impedance potentiostatic: require... <a href="#">...</a>	
End status Autolab	<a href="#">...</a>	
Signal sampler	No signals. <a href="#">...</a>	
Options	1 Options <a href="#">...</a>	
Instrument	$\mu 3AUT71176$	
Instrument description		
Timed procedure		
Autolab control	<a href="#">...</a>	
Set potential	0.002	
Set cell	On	<a href="#">...</a>
Wait time (s)	5	
<..>		
FRA measurement potentiostatic		
Frequency	<..array..> (Hz)	
Phase	<..array..> (°)	
Time	<..array..> (s)	
Z	<..array..> ( $\Omega$ )	
Z'	<..array..> ( $\Omega$ )	
Z''	<..array..> ( $\Omega$ )	
Index	<..array..>	
FRA frequency scan <a href="#">...</a>		
Integration time (s)	0.125	
Minimum number of cycle...	1	
Number of frequencies	50	
Estimated duration	13m	
FRA single frequency	[0.125, 1, 10, 1, 0]	
<..>		
Build signal	<a href="#">...</a>	
Nyquist -Z'' vs Z'	<a href="#">...</a>	
Bode modulus	<a href="#">...</a>	
Bode phase	<a href="#">...</a>	
<..>		
Timed procedure		
Set cell	Off	<a href="#">...</a>
<..>		

Figure 2.11 FRA impedance potentiostatic procedures.

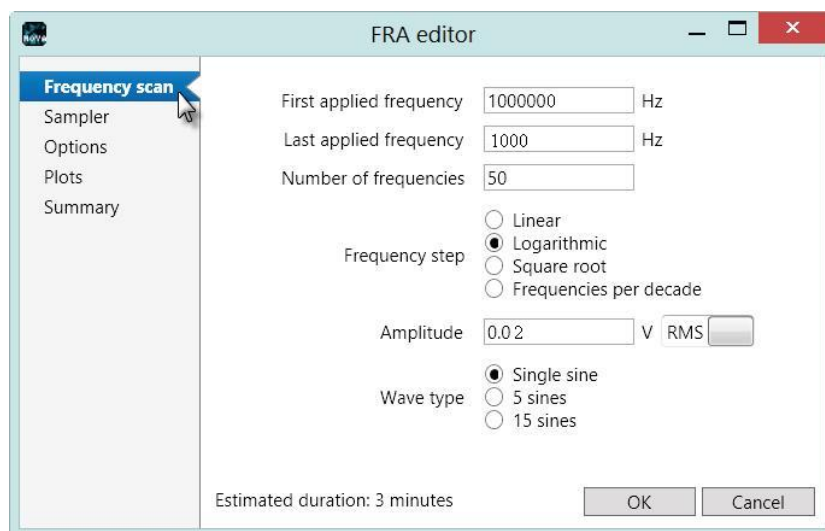


Figure 2.12 Frequency set.

In a nyquist plot, the intersection of the impedance data with the real part of the axis at the high frequency end gives the ohmic resistance shown in Figure 2.13.

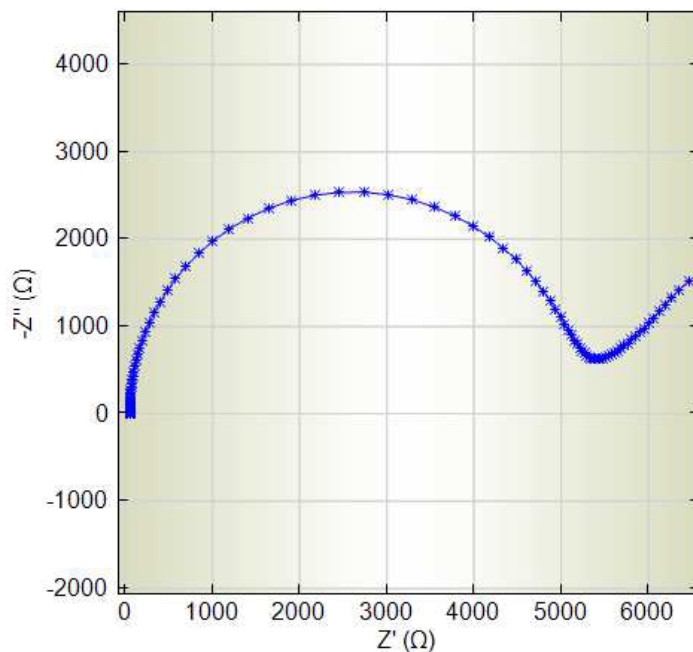


Figure 2.13 A standard nyquist plot.

The ionic conductivity is calculated using

$$\sigma = \frac{l}{RA}, \quad (2)$$

where,  $l$  is the membrane thickness, cm,  $R$  is the ohmic resistance, ohm, and  $A$  is the membrane surface area, cm<sup>2</sup>.

#### 2.4.2 Dynamic Mechanical Analysis

Stress/strain measurements are widely used to characterize films over a broad range of viscoelastic behavior. Although conventional physical testing devices can accommodate thin films, the results are difficult to obtain, and the accuracy is doubtful since the mass and inertia of the grips are much greater than the tensile strength of the material being evaluated. The clamping arrangements and force range of DMA shown in Figure 2.14 are more suitable for examining polymeric films.

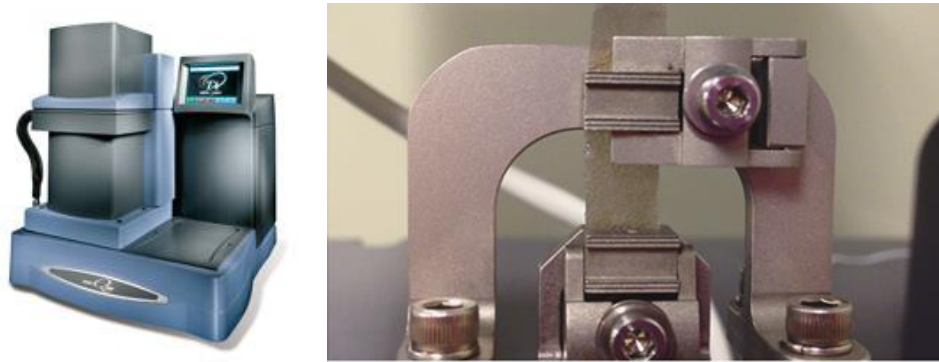


Figure 2.14 Stress/strain measurements.



Summary Procedure Notes

Procedure Information

Test: Strain Ramp

Notes: Sample is exposed to a constant strain-rate while the temperature is held isothermal.

Strain Rate

Preload force: 0.0020 N Advanced...

☒ Initial Strain : 0.1000 % Post Test...

☐ Initial Displacement : 0.0000  $\mu\text{m}$

Isothermal temperature: 25.00  $^{\circ}\text{C}$

Strain Rate: 50.00 %/min

Final Strain: 100.000 %

Figure 2.15 Strain rate procedures.

Figure 2.15 shows the settings of the DMA test. The value of the preload force is based on the film itself. To choose the right values, we need to start from the lowest one usually 0.001.

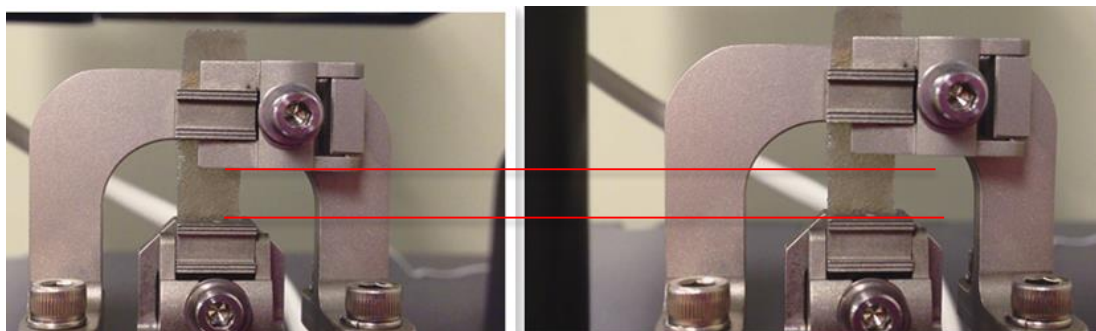


Figure 2.16 The elongation of the film during the DMA tensile test.

The elongation of the film during the DMA tensile testing is shown in Figure 2.16. In some cases, the film may break before it reaches the maximum strain. It depends on the quality of the films. Bubbles or flaws can degrade the mechanical properties.

### **2.4.3 Differential Scanning Calorimetry**

The DSC is used to detect a material's phase transitions by monitoring the difference in power or heat supplied to maintain two sample containers at the same temperature. One container holds the material under the investigation, and the other is empty used as the reference container. Both DSC containers are heated and cooled at the same rate. Since melting is an endothermic process, when a crystalline or semi-crystalline sample melts, more power or heat is needed to maintain the temperature of the sample. Conversely, less power or heat is required to maintain the temperature when crystallization occurs. By plotting the heat flow as a function of time, we can identify the temperature of the phase transitions.

Differential scanning calorimetry (DSC) measurements were made on all samples carried out under nitrogen atmosphere with a TA Instruments Q2000 DSC. The weight of the sample and that of the Tzero aluminum container pans and lids were taken before and after each thermal scan. The sample was heated to 200°C, cooled to -90°C and heated to 200°C again with heating and cooling rates of 10°C/min and 5°C/min (Fig 2.17). The glass transition temperature was determined as the mid-point of the step transition from the second heating. Melting and crystallization temperatures (when observed) were defined as the maxima of the melting endotherms and crystallization exotherms, respectively.

The screenshot shows a software window with three tabs: 'Summary', 'Procedure', and 'Notes'. The 'Procedure' tab is active. It contains two main sections: 'Procedure Information' and 'Method'.

**Procedure Information:**

- Test:** A dropdown menu set to 'Heat/Cool/Heat'.
- Description:** A text box containing the text: 'Material is heated at a linear rate to an elevated temperature to erase previous thermal history, then cooled at a linear rate before heating again.'

**Method:**

- Start temperature:** A checkbox labeled 'Use current' is unchecked. Next to it is a text box with '30.00' and a unit label '°C'. To the right are two buttons: 'Advanced...' and 'Post Test...'.
- Heating rate:** A text box with '10.000' and a unit label '°C/min'.
- Upper temperature:** A text box with '200.00' and a unit label '°C'.
- Cooling rate:** A text box with '5.000' and a unit label '°C/min'.
- Lower temperature:** A text box with '-90.00' and a unit label '°C'.

Figure 2.17 The DSC heat/cool/heat procedure.

#### 2.4.4 Scanning Electron Microscope

The scanning electron microscopy (SEM) has been the most widely used instrument to characterize the morphology and topology of different samples especially at nanoscale. The surface morphologies and cross sections of the GO nanocomposite electrolyte were investigated using SEM. Figure 2.18 shows the polymer nanocomposite electrolyte samples on a carbon tape pasted onto SEM mounts.



Figure 2.18 Polymer nanocomposite electrolyte samples.

#### 2.4.5 Fourier Transform Infrared Spectroscopy

Fourier Transform Infrared (FTIR) spectroscopy was conducted to determine the effectiveness of additives in promoting dissociation of  $\text{LiClO}_4$  in solid polymer electrolytes. FTIR applications encompass the necessity for detailed information regarding chemical composition of the items in question, yielding a broad range of applications from analysis of lithium-ion battery components. In this study, we analyzed the addition of graphene oxide (GO) into poly (ethylene oxide) solid polymer electrolyte to observe its effects on the dissociation of  $\text{LiClO}_4$ .

Three samples were taken from different areas of the polymer and placed in the FTIR for measurement. Once the sample is taken with the MicroLab software, the collected data and spectrum plot is opened in Resolutions Pro for analysis. In order to determine percent dissociation, the area underneath the curve is taken within the  $620\text{-}624\text{ cm}^{-1}$  range to obtain the amount of dissociated  $\text{ClO}_4^{-1}$  as well as the area under the curve within the  $630\text{-}635\text{ cm}^{-1}$  range, as this range represents  $\text{LiClO}_4$  [29][30].

## Chapter 3 Results and Discussions

### 3.1 Ion Conductivity

Previous studies have shown that the ion conductivity can be enhanced by two to three orders of magnitude at room temperature when nano-sized ceramic fillers are added to a polymer–lithium salt complex [20, 31]. The present study focuses on the role and the enhancement mechanism of nano-sized fillers at room temperature from two main points, the dielectric properties and the degree of crystallization [32]. The conductivity of a solid-state electrolyte has many determinants, such as carrier concentration, mobility and other [33]. Figure 3.1 Nyquist plot of GO based polymer nanocomposite electrolytes. It may be clearly seen that the amplitude of the middle-frequency semicircle shows a substantial progressive increase upon storage. This is a clear indication of a progressive increase of the interfacial resistance and thus, of a continuous growth of the passivation layer. We measured at least three samples for each concentration and table 3.1 is the results of complex impedance spectroscopy. For 8% GO we only get few samples which are ionic conductive. Due to the serious aggregation, the ions were probably trapped in the aggregated GO “cages” in the polymer matrix and were immobilized.

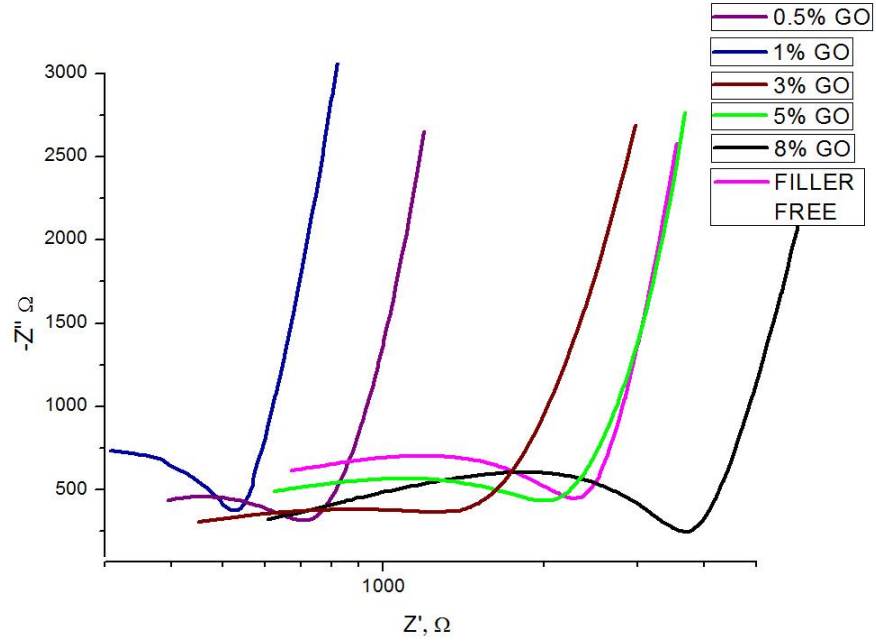


Figure 3.1 Nyquist plot of GO based polymer nanocomposite electrolytes.

Table 3.1 Complex impedance spectroscopy results.

Electrolyte type	Thickness (mm)	Area (cm <sup>2</sup> )	$Z''$ (Ω)	Ohmic Resistance $Z'$ (Ω)
PEO without filler	0.26	1134.12	669.74	2463.93
	0.25		766.43	2513.37
	0.26		782.71	3166.58
0.5% GO filled	0.26	1134.12	154.53	685.12
	0.28		195.98	828.78
	0.29		184.53	768.43
1% GO filled	0.31	1134.12	45.91	344.21
	0.30		55.23	493.72
	0.28		99.16	645.44
3% GO filled	0.31	1134.12	390.83	1045.43
	0.27		459.43	1453.13
	0.23		460.90	1800.58
5% GO filled	0.24	1134.12	575.95	1922.28
	0.29		770.24	2458.81
	0.25		809.72	2976.19
8% go filled	0.29	1134.12	1081.84	4336.19
	0.31		N/A	N/A
	0.32		N/A	N/A

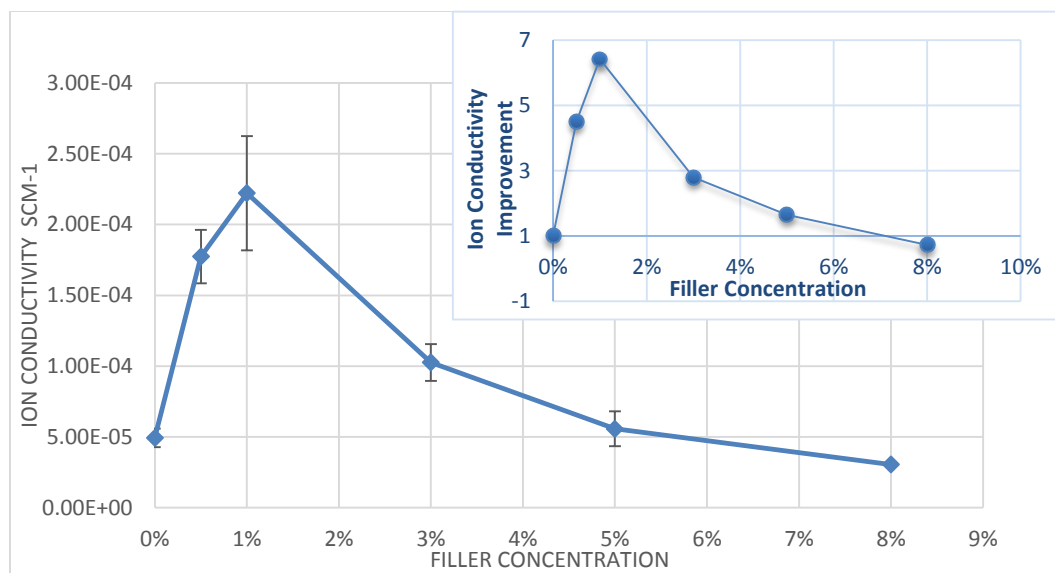


Figure 3.2 Relationship between ionic conductivity and filler concentration and relationship between ionic conductivity improvement and filler concentration.

All measurements have associated variability. We systematically prepared and measured the conductivity values for the same sample type at least 3 times and the error bars were calculated using the normal distribution. The addition of graphene oxide observably improved ion conductivity (Fig.3.2) similar to the effects of other ceramic fillers (Table 3.2).

Table 3.2 Ion conductivity reported from other fillers at room temperature [20].

Class of polymer electrolyte	Conductivity (S cm <sup>-1</sup> )
PEO-based SPEs (pure)	10 <sup>-7</sup>
Inert oxide ceramic	3.8 × 10 <sup>-4</sup>
Treated SiO <sub>2</sub>	2.3 × 10 <sup>-5</sup>

Table 3.3 Ion conductivity reported from other fillers at room temperature [20],  
(continued).

Class of polymer electrolyte	Conductivity ( $S\ cm^{-1}$ )
Molecular sieves or zeolite	$1.4 \times 10^{-5}$
Rare-earth ceramics	$3.8 \times 10^{-4}$
Solid super acid	$2.1 \times 10^{-5}$
Ferroelectric material	$2.6 \times 10^{-5}$ <sup>b</sup>
Cellulose nanocrystals	$10^{-5}$

<sup>b</sup>: measured at 30 °C.

The data shows that the ionic conductivity of filler-inserted electrolyte has a maximum of  $2.67E-4\ S\ cm^{-1}$  at ambient temperature when GO is added at about 1 wt. %. The enhancement in ionic conductivity, when adding a high dielectric ceramic filler ( $TiO_2$ ,  $BaTiO_3$ ,  $PbTiO_3$ , etc.) to a PEO–Li salt complex, might be mainly associated with free volume expansion and higher mobility due to reduced crystallinity and partially associated with increased concentration of mobile carriers due to active dissociation of the Li salt [16]. This theory does not hold exactly same for the present use of GO, however, as this material has a special structure, we may discuss it from the constitution of PEO/GO nanocomposite polymer electrolyte.



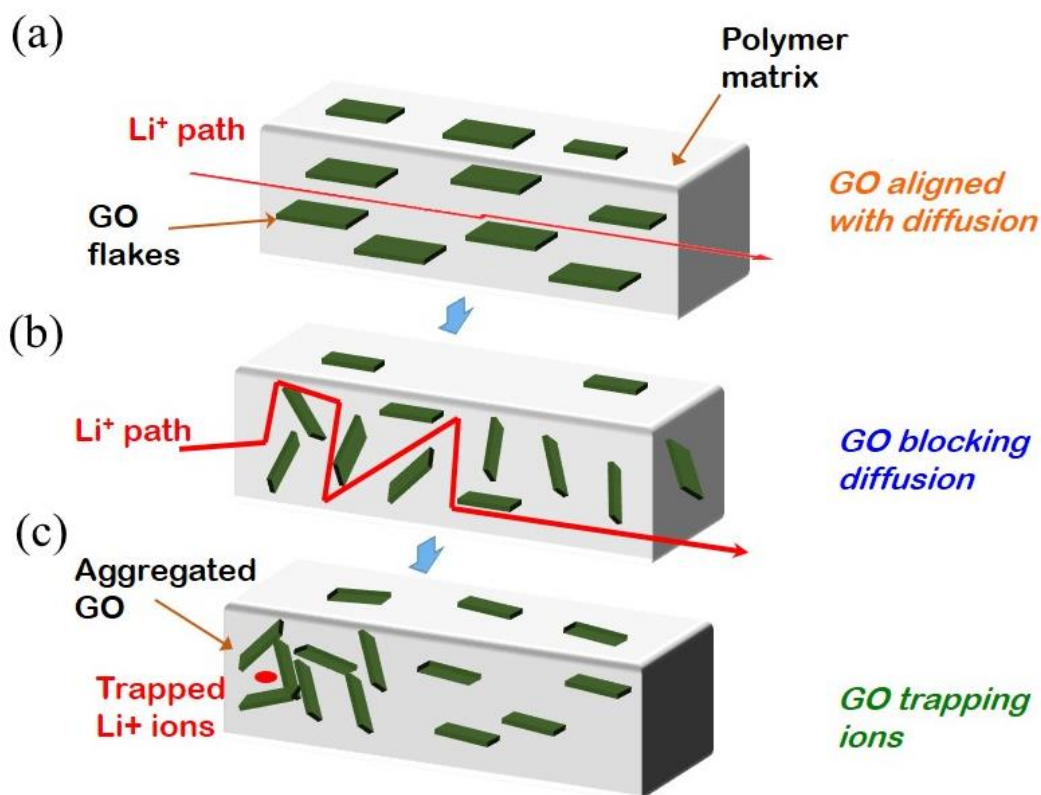


Figure 3.3 GO fillers (a) aligned with diffusion (b) blocking diffusion and (c) trapping ions.

The graphene oxide itself has a very large aspect ratio which leads to aggregation. Chemically, GO has plenty of oxygen atoms on the graphitic backbone in the forms of epoxy, hydroxyl, and carboxyl groups [34]. These oxygen groups can bind to metal ions. The folding and aggregation of GO should be initially driven by the interaction between GO and  $\text{Li}^+$ . The interaction of  $\text{Li}^+$  with GO most likely happens at the oxygen sites, because the skeleton carbon has much lower affinity to metal ions than oxygen atoms do [35]. At low contents, this effect may not impede ion conductivity. The slight aggregation may be counteracted by large improvement of ion transportation. In an ideal model graphene oxide sheets formed paths for ions to transport in solid polymer electrolyte matrix

(Fig.3.3a). When more graphene oxide sheets are added, they tend to aggregate instead of forming paths (Fig.3.3b). At some point (according to our experiments 5 wt. % as shown in Fig.3.2) the GO sheets are significantly stacked and wrinkled. The term “stacking” refers to the parallel packing of the GO sheets and “wrinkling” refers to the localized folding of a flat GO sheet [36]. The stacking and wrinkling in the GO aggregates can significantly block and trap the Li ions (Fig.3.3c). In this situation, the GO fillers can actually impede the ion conduction.

### 3.2 Mechanical Property and Application (Stress/Strain Rate)

The stress/strain curves for the polymer electrolytes are presented in Figure 3.2.1. The 1 wt. % electrolyte film has a critical stress of 1.272 MPa with an elongation-at-break value of 15.78%.

Stress–strain measurements showed a large enhancement of the Young's modulus and of the yield-point stress when passing from filler-free to nanocomposite polymer electrolytes. Here, the active nanocomposite particles serve as both filler and “tie molecules,” thus improving the adhesion between polymer chains.

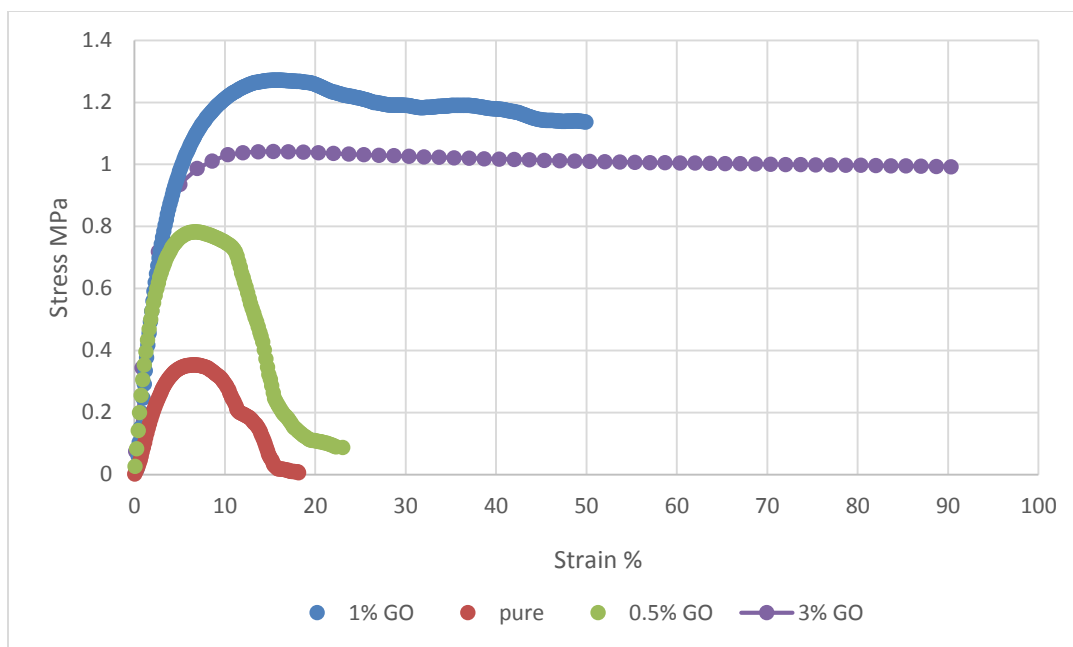


Figure 3.4 Comparison of Stress/Strain curves of electrolyte films.

Previous research has indicated that the conductivity state of the ion transportation is not due to polymer degradation but rather is accompanied by a substantial increase in the electrolyte's mechanical properties[19]. These results indicate that the PEO/GO membrane at lower GO contents (i.e, 0.5% and 1%) exhibits superior tensile strength while the % elongation remains uncompromised. The filled polymer becomes slightly more brittle than the pure PEO polymer and the Young's modulus increases. This may be caused by the GO sheets mechanical properties which can increase both the tensile strength and elastic modulus in the polymer nanocomposite material.

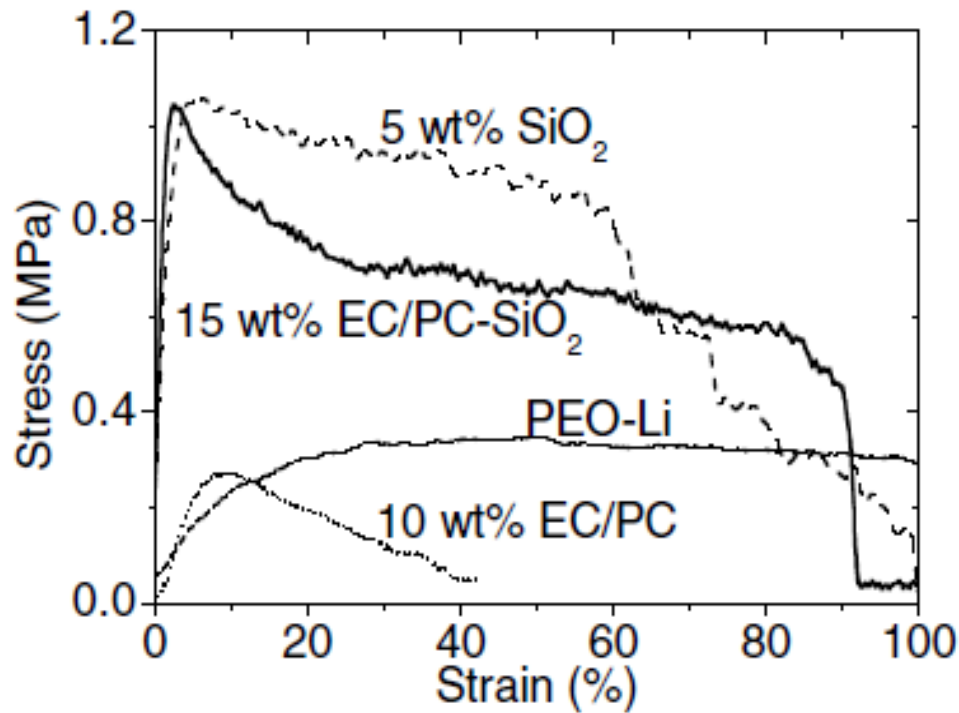


Figure 3.5 A Comparison of the tensile Stress-Strain curves measured for the PEO-Li based electrolyte films [37].

The mechanical properties of polymers can be further improved by uniform dispersion of nanoparticles into the polymer matrix. The properties of the nanoparticles are tied at the interface of the polymer and filler. Figure 3.3 shows a previous research about the strain/stress rate dependence on nanoparticles [37]. Since the GO filler has extremely high specific surface area, most of the polymer is present at the interface. If the interaction at the interface is a strong one, or if the structure of the interfacial polymer is very different from the bulk, it is possible to see different properties in the material as a whole. These changes have a fundamentally different origin than those found in micro- and macro-composites, where the volume of the interphase is only a small fraction of the overall volume of the material. The mechanical properties are potentially superior to fiber-

reinforced polymers because reinforcement from the inorganic layers occurs in two dimensions without special efforts to laminate the composites.

### 3.3 Thermal Analysis

In the absence of  $\text{LiClO}_4$ , 78% of the pure PEO sample crystallizes at 60°C. The crystalline fraction represents the fraction of the sample occupied by crystalline lamellae. The addition of  $\text{LiClO}_4$  decreases the fraction of crystalline lamellae and depresses the melting point.  $T_g$  is the glass transition temperature of the amorphous polymer regions surrounding the spherulites. The value of  $T_g$  is increased markedly by  $\text{LiClO}_4$  via the so-called “salt effect.” The presence of  $\text{Li}^+$  salt, can be attributed to a reduction in flexibility of the polymer chains due to the interaction between the ether oxygens of the polymer chains and the  $\text{Li}^+$  ions [38]. The fraction of crystalline PEO is a function of lithium concentration, and so is the  $T_g$ . The ratio of the polymer to salt (O:Li) in our experiment is 16:1. According to our DCS result the  $T_g$  is -25.3 °C,  $T_c$  is 28.13 °C,  $T_m$  is 59.89 °C.

In general, a low glass transition temperature indicates the existence of a greater amount of amorphous phase such that the segmental motion of migrating lithium ions is more activated [32].  $T_g$  increases with increasing lithium concentration indicating decreased polymer mobility. The nanoparticles become the “knots” of the re-crystallization of polymer molecular chains and thus the polymer molecular chains are disarranged, as the crystallites in the amorphous phase can act as physical crosslinks and thereby increase  $T_g$  [39]. Filler additions in PEO-salt lower the crystallinity by increasing the volume fraction of amorphous phase, caused by distortion of the polymer structure. Figure 3.6 shows the trace of DSC test, and Figure 3.7 gives the relationship between the  $T_g$  and GO concentration.

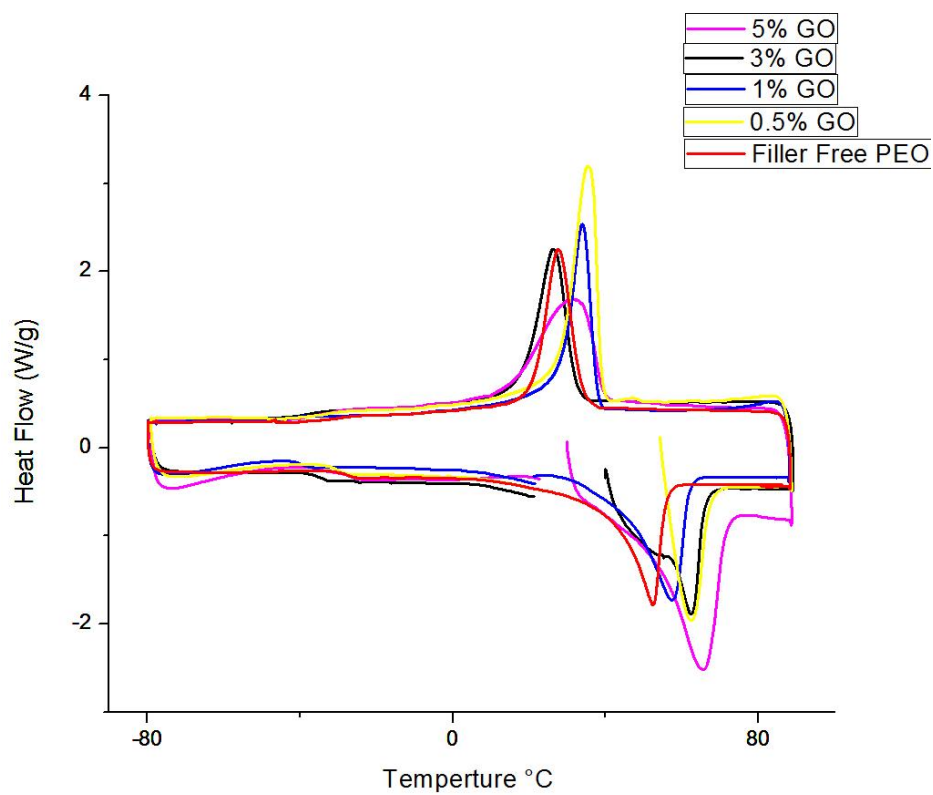


Figure 3.6 DSC traces as a function of graphene oxide concentration.

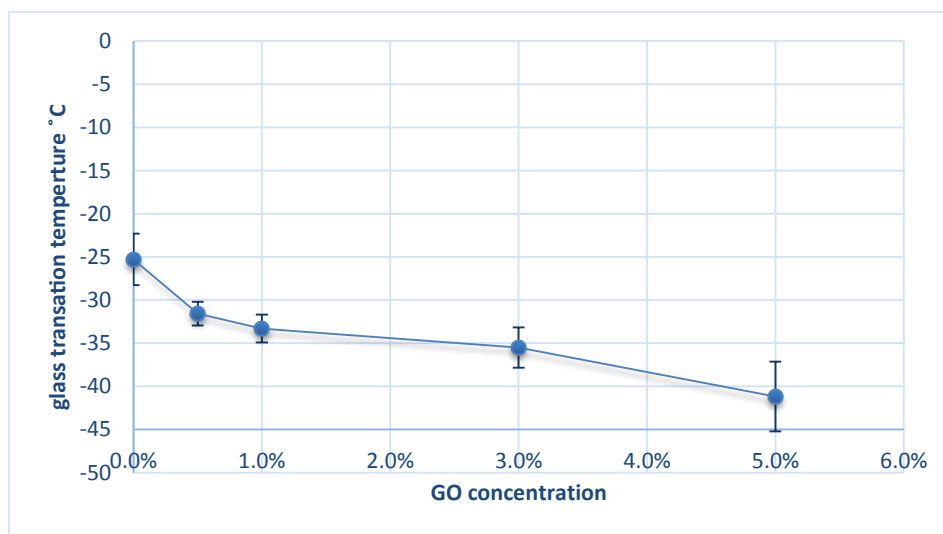


Figure 3.7 The relationship between glass transition temperature and GO concentration.

Through both figures, it can be seen that the GO fillers decrease the  $T_g$  of PEO effectively. The lowest  $T_g$  of about  $-35^\circ\text{C}$  is obtained when the content of ranges from 1 to 3 wt. % of PEO weight. The decrease of  $T_g$  will increase the flexibility of the PEO chains and the ratio of amorphous state PEO, respectively. As a result, the ionic conductivity should be enhanced at low temperature regions. Even though we have lower  $T_g$  at 5 wt. %, the GO aggregation may have blocked ions diffusion paths and trapped the Li ions leading to decrease in ion conductivity instead.

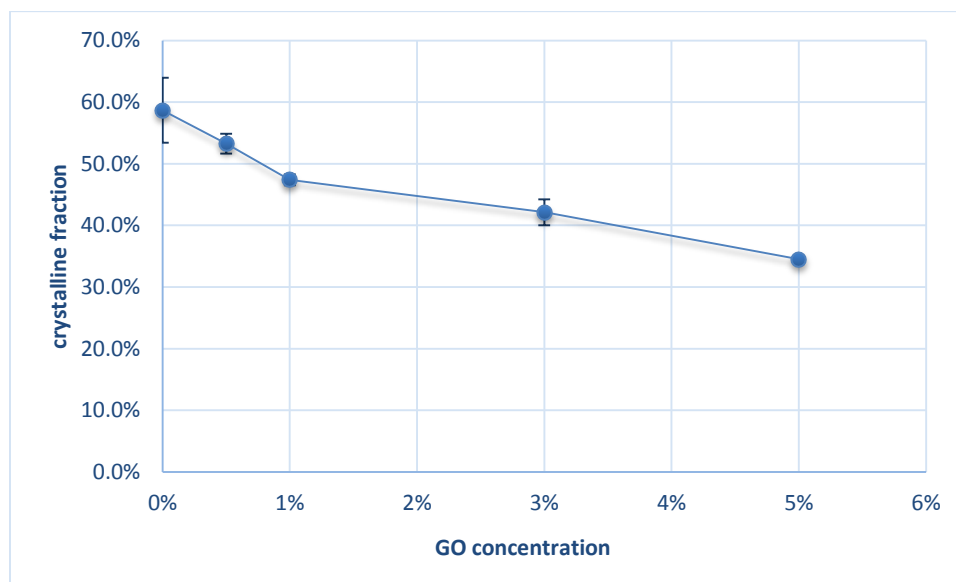


Figure 3.8 PEO crystalline fraction as a function of GO concentration for all samples.

$T_c$  provides an index of the thermal stability of the amorphous state. During the fractional crystallization of PEO component, the broad  $T_c$  could induce the formation of PEO crystals with less uniform morphology and perfectness [40]. Therefore, all of the blends show much broader melting peaks than the neat PEO [41]. We report the PEO crystalline fraction  $[\chi_c]$  in Figure 3.8 as a function of nanoparticle concentration. The crystalline fraction  $[\chi_c]$  can be calculated from the following equation [42]:

$$\chi_c = \left( \frac{\Delta H_m}{\Delta H_m^0} \right) \times 100\%, \quad (3)$$

where,

$\Delta H_m$ : the fusion heat of PEO/Li-xGO (x=0, 0.5%, 1%, 3%, 5%),

$\Delta H_m^0$ : the melting heat of pure PEO crystalline, 216 J/g (100% crystalline).

The fusion heat  $\Delta H_m$  can be calculated from the integral area of the DSC curves. The crystalline fraction  $\chi_c$  is summarized in Table 3.3. The decrease in crystallinity is also manifested as the decrease in glass transition temperature. In the case of filler free PEO the crystallinity gradually decreases with an increase in GO loading because of the steric hindrance caused by the huge surface area of randomly oriented graphene oxide sheets throughout the matrix.

Table 3.4 DSC thermal properties of solid polymer electrolyte in our study.

Type	T <sub>g</sub> , °C	$\chi_c$	T <sub>m</sub> , °C
Pure PEO	-54.21	N/A	66.48
PEO Li Salt Without Filler	-25.3	58.7%	59.88
0.5% GO/PEO-Li	-31.58	53.3%	63.75
1% GO/PEO-Li	-33.31	47.4%	60.47
3% GO/PEO-Li	-37.42	42.1%	63.30
5% GO/PEO-Li	-41.52	34.5%	59.03

In a semicrystalline PEO-salt polymer, T<sub>m</sub> is the melting temperature of spherulite.

Table 3.3 shows the comparison between the T<sub>m</sub> of pure PEO and different concentration fillers. The melting temperature (T<sub>m</sub>) and crystalline temperature (T<sub>c</sub>) of PEO is decreased when the Li salt is introduced into the PEO matrix as seen in the previous studies [43]. This



can be explained through the coordination interactions between the ether O atoms of PEO chains and  $\text{Li}^+$  cations, which can inhibit the reorganization of PEO chains effectively and hence decrease the recrystallization of PEO [44]. Normally,  $T_m$  depends on the molecular weight of the polymer. Introducing GO fillers which act as thermal insulators into polymer matrix, may ideally increase the melting point. As it can be seen from Table 3.3, the addition of GO does slightly increase the  $T_m$ . However, the trend is not uniform and fluctuation in the  $T_m$  is observed. This may be due to GO aggregation and non-uniformity of the samples, especially at high GO concentrations.

### 3.4 Morphology

The morphology study of the polymer nanocomposite electrolyte can reveal the crystalline and amorphous polymer phases, material defects and the shape, size and dispersion properties of the additives. The macro-scale pictures of the fabricated PEO/GO membranes in petri dishes were shown in the previous section on the preparation methodology (Fig. 2.8). The color and texture changes in the polymer with the added GO fillers were observed previously. The macro-sized photos showed no obvious processing defects such as air bubbles or macropores, however filler aggregation has been observed.

The SEM image of filler free PEO-Li electrolyte (Fig. 3.9) shows distinct spherulites indicative of the lamellar microstructure of the pure polymer. The pure PEO film reveals a semi-crystalline structure. The formation of the crystalline structures in PEO can be linked to the solvent evaporation durations [45] and temperatures.

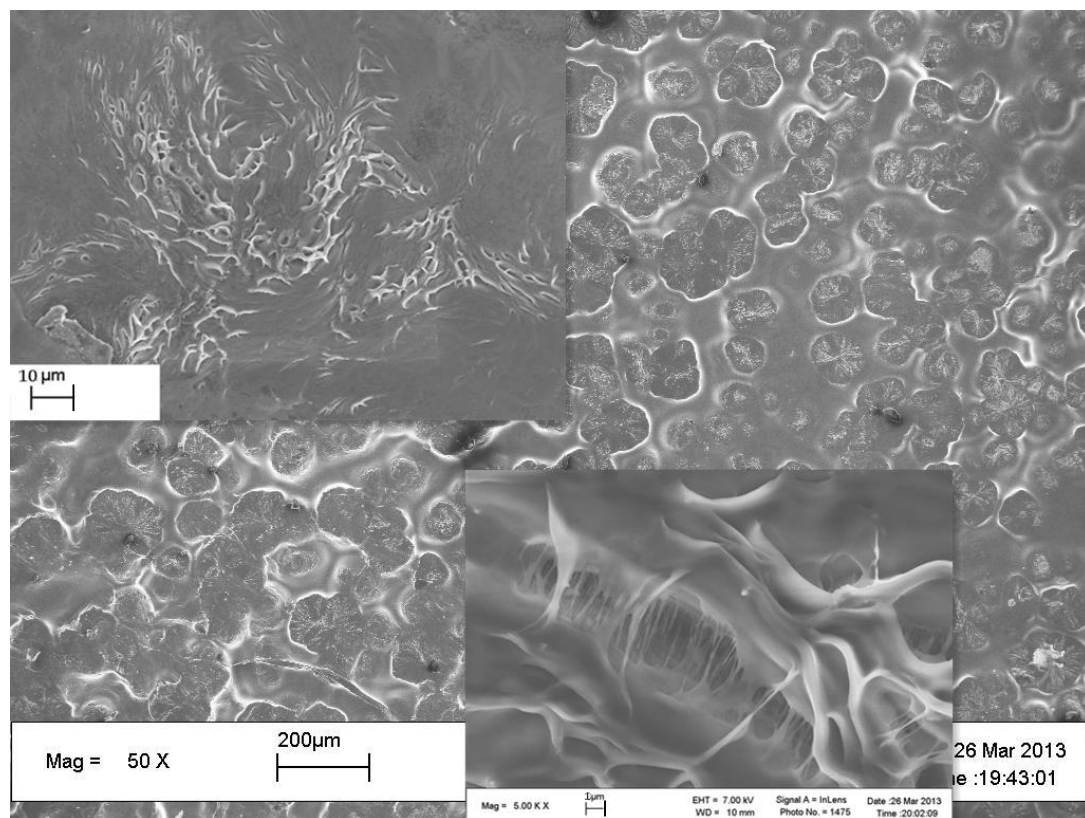


Figure 3.9 SEM picture of pure PEO-Li polymer electrolyte.

The SEM images of the PEO/GO films of various GO contents are shown in Figure 3.10. The images reveal the characteristics of amorphous and crystalline regions in the polymer composite at micron and nano-scales. It is clear that the filler-free PEO has a rough surface consisting of spherulites of an almost equal size with several crystalline domains.

GO is highly hydrophilic as expected from its high oxygen content in the inter-lamellar regions [46]. It can accommodate water or other solvent molecules between its layers with a surprisingly high degree of long-range order [47, 48]. Compared to the filler-free PEO film, the filled GO/PEO films with 0.5 wt. %, 1 wt. % and 5 wt. % contents show that the addition of the graphene oxide prominently attenuates the crystallization of PEO matrix which can lead to improvement in Li ion mobility.

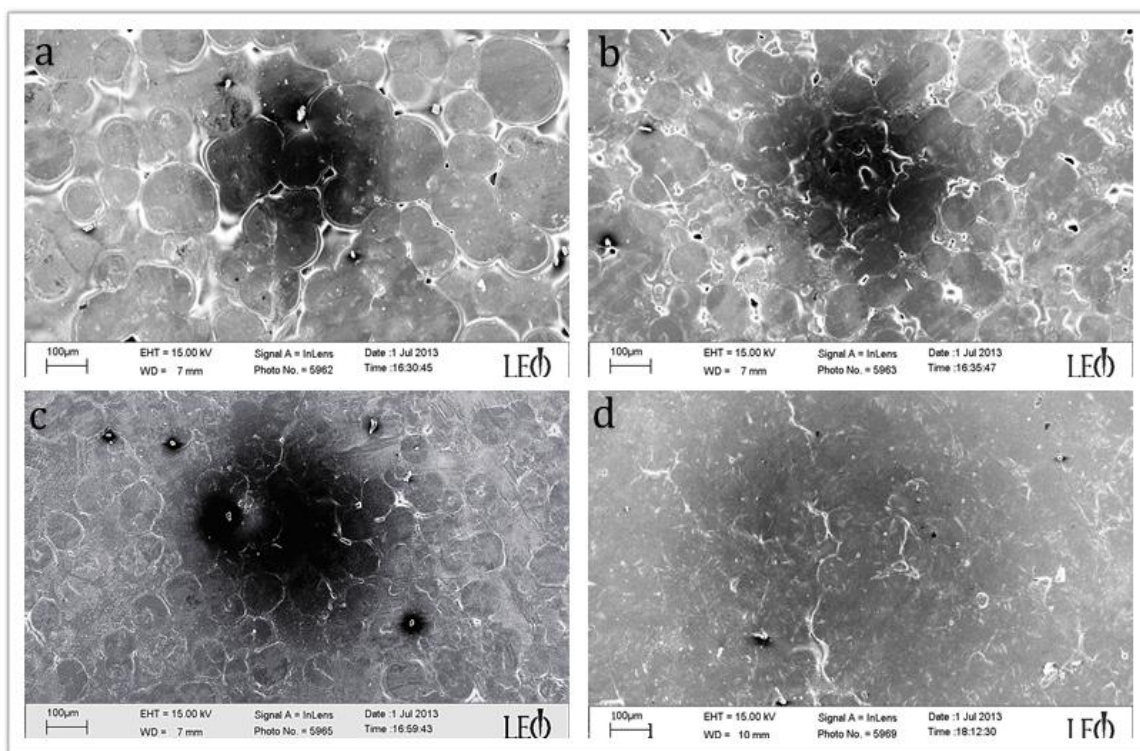


Figure 3.10 SEM image of (a) Filler Free polymer electrolyte (b) 0.5 wt. % GO (c) 1wt. % GO (d) 5wt. % GO/PEO-Li polymer electrolyte.

The high-magnification SEM image in Figure 3.11 reveals that the GO consists of a thin wrinkled paper-like structure. The cross-sectional morphology of the 1 wt% GO/PEO Li film is shown in Figure 3.12 exhibiting a wavy structure. The fabricated polymer membranes were about 100-200  $\mu\text{m}$  thick and the intrinsic ripples of GO nanosheets may have contributed to the wavy structures in the macroscopic scale (Figure 3.12). The graphene oxide size is about 0.5-5 microns in length and width and about  $1.1 \pm 0.2$  nm in thickness. A hint of the lamellar structure at the edges of flakes can be seen from the cross-sectional SEM image.

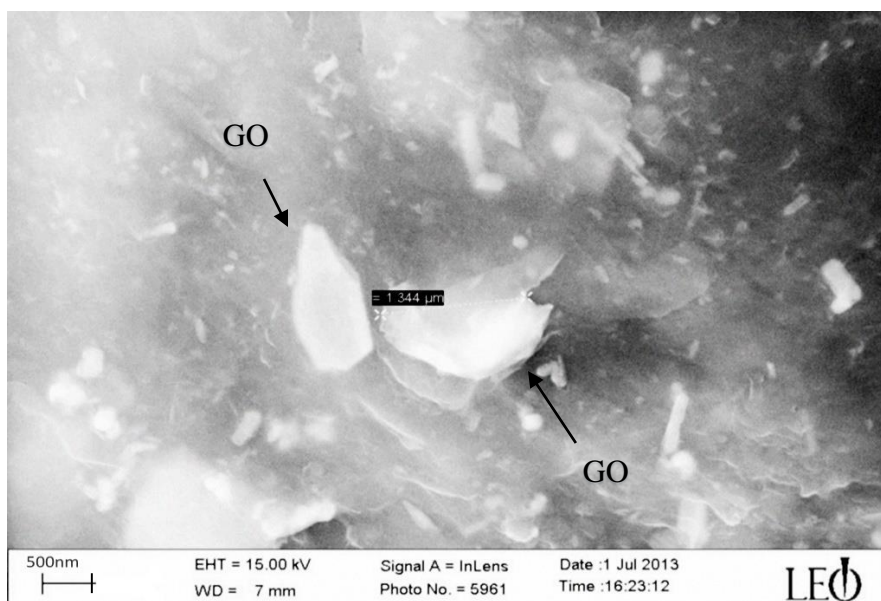


Figure 3.11 SEM picture of 1 wt. % GO/PEO-Li polymer electrolyte.

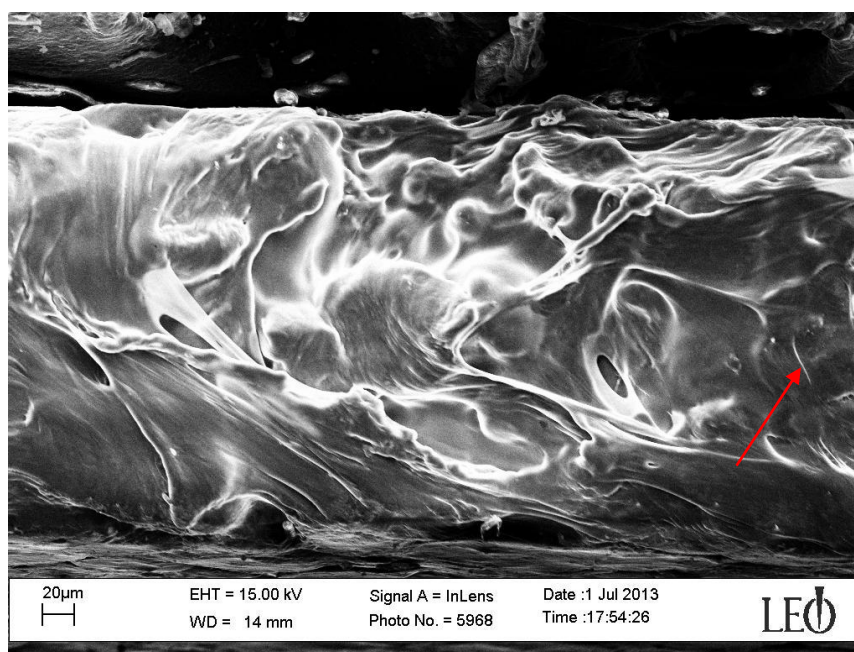


Figure 3.12 SEM image of cross sectional morphology of 1 wt. % GO/PEO-Li polymer electrolyte.

### 3.5 Fourier Transform Infrared Spectroscopy

Figure 3.13, shows the FTIR spectra for samples representing filler free polymer electrolyte, 0.5 wt. % GO, 1% GO, and 3% GO. The figure demonstrates that each spectra peaks at the 620-624  $\text{cm}^{-1}$  range, representing the dissociation of  $\text{LiClO}_4$  [30]. The percent dissociation is calculated from Equation below:

$$\frac{A}{A+B}, \quad (4)$$

where A: the area underneath the  $\text{ClO}_4^{-1}$  range and B: the area underneath the  $\text{LiClO}_4$  range.

Each spectrum chosen in the figure represents the sample whose fraction of dissociation most closely reflects that of the average of all samples from each species. It also shows that each spectrum peaks around 622  $\text{cm}^{-1}$ , and each peak rises between 0.35 and 0.4 from its baseline of reflectance. The similarity between peak heights for all four of the spectra suggests an equal amount of dissociation between the four species of polymer.

Figure 3.14 shows the % salt dissociation averages of pure and filled polymer species using FTIR including error bars to demonstrate measurement variability. This plot shows that the average dissociation fractions for each polymer species lay within 0.015 of each other, suggesting little change in dissociation of  $\text{LiClO}_4$  with increase in percent GO content. Therefore, the increase in ion conductivity observed at lower GO percentages is postulated to be mainly due to free volume expansion in the polymer nanocomposite electrolyte and not directly associated with salt dissociation.

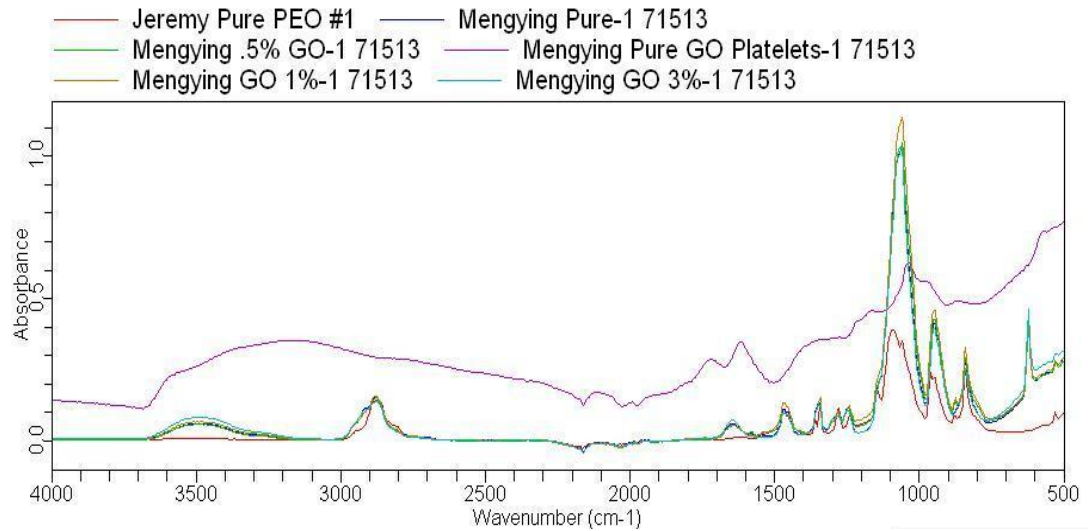


Figure 3.13 FTIR spectra of pure GO, pure PEO, filler free, 0.5% GO, 1% GO and 3% GO polymer electrolytes.

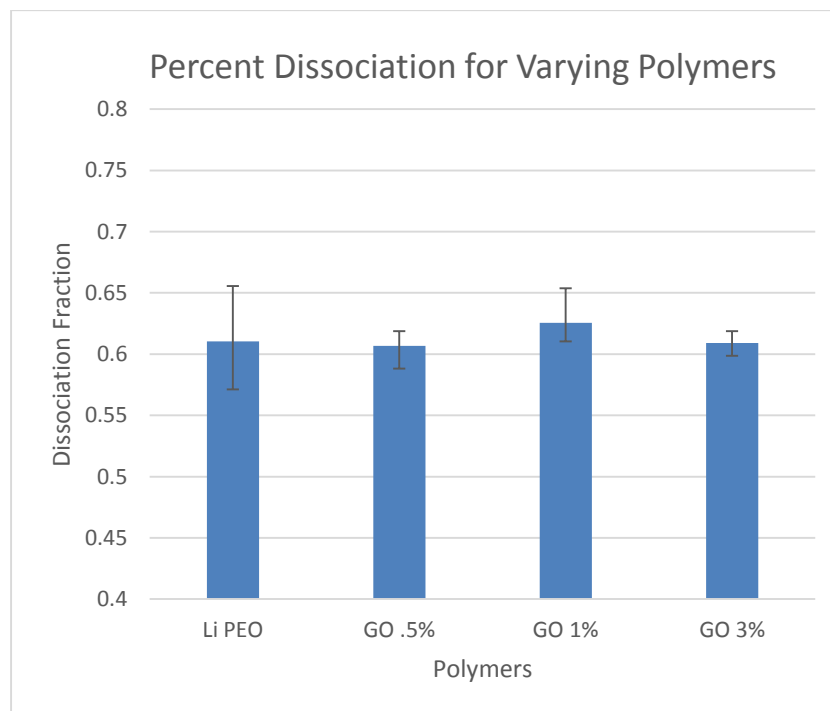


Figure 3.14 Li salt dissociation fractions of pure and filled polymer species from FTIR.

## Chapter 4 Conclusions and Summary

### 4.1 Conclusions

The following conclusion statements can be made in this study:

- 1) Graphene oxide sheets can improve the Li ion conductivity of solid polymer electrolyte for lithium-ion battery up to  $2.67\text{E-}4 \text{ S cm}^{-1}$  at room temperature which is about one order of magnitude improvement from our measured filler free PEO conductivity and about 3 orders of magnitude higher than the typically published conductivities ( $10^{-7} \text{ S cm}^{-1}$ ) of filler free PEO polymer electrolyte.
- 2) The mechanical properties including tensile strength of the GO filled PEO are enhanced. The active graphene oxide nanocomposite particles serve as both filler and tie molecules, improving the adhesion between polymer chains. The % elongation of the GO/PEO at lower GO contents appears uncompromised. PEO/GO electrolyte film with only 1 wt. % GO can exhibit a critical stress of 1.272 MPa with an elongation-at-break value of 15.78%.
- 3) Based on the DSC results, GO fillers appear to disrupt the crystalline formation in the semi-crystalline PEO leading to expansion in free volume supported by the observed reductions in  $T_g$  and % crystallinity. This can explain the improvement in Li ion conductivity at lower filler contents.
- 4) SEM results provide the structural evidence that graphene oxide reduces the crystallization of PEO matrix effectively.

- 5) FTIR results suggest that the dissociation of Li ions in PEO was not significantly affected by the presence of GO fillers. Therefore, the ion conductivity improvement is mainly attributed to the polymer morphological and structural changes affecting Li ion mobility.

## 4.2 Summary

In this work, the graphene oxide based solid polymer nanocomposite electrolyte was investigated for lithium-ion battery. Electrochemical, mechanical and thermal measurements were used to study this novel solid polymer electrolyte. The GO-PEO electrolytes appear to exhibit promise of improved ion conductivity and mechanical properties and can be considered for special applications such as flexible Li ion batteries.

Future work should be mainly focused on solving the aggregation of the graphene oxide sheets. According to our results, the high concentration of graphene oxide impedes the ion transport in a polymer matrix due to the aggregate of fillers. However, both the microstructure and thermal properties show a significant reduction of crystallization in high content filler which is very promising for further increase in ion conductivity.



## References

- [1] Tarascon, J. M., and Armand, M., 2001, "Issues and Challenges Facing Rechargeable Lithium Batteries," *Nature*, 414(6861), pp. 359-367.
- [2] Linden, D., 1995, *Handbook of Batteries*, McGraw-Hill, New York.
- [3] Cheung, I., 2006, "The Physical and Electrochemical Characterization of New Lithium-ion Conducting Polymer Electrolytes," Dissertation/Thesis, Proquest, UMI Dissertations Publishing.
- [4] Cross, J., 2010, "White Paper: Rechargeable Batteries," [http://www.maximumpc.com/article/features/white\\_paper\\_rechargeable\\_batteries](http://www.maximumpc.com/article/features/white_paper_rechargeable_batteries).
- [5] Meyer, W. H., 1998, "Polymer Electrolytes for Lithium-ion Batteries," *Advanced Materials* (Deerfield Beach, Fla.), 10(6), pp. 439-439.
- [6] Shirey, S. K. F., 2009, "A Unified Approach to Understanding Conductivity Enhancement in Nanoparticle-Filled Solid Polymer Electrolytes for Lithium-Ion Batteries," Doctor of Philosophy, The Pennsylvania State University.
- [7] Yuan, X., Liu, H., and Zhang, J., 2012, *Lithium-ion Batteries: Advanced Materials and Technologies*, CRC Press, Boca Raton.
- [8] Xu, K., 2004, "Nonaqueous Liquid Electrolytes for Lithium-based Rechargeable Batteries," *Chemical Reviews*, 104(10), pp. 4303-4417.
- [9] Fenton, D. E., Parker, J. M., and Wright, P. V., 1973, "Complexes of Alkali-Metal Ions with Poly(Ethylene Oxide)," *Polymer*, 14(11), pp. 589-589.
- [10] Armand, M. B., Chabagno, J. M., and Duclot, M., 1978, "Second International Meeting on Solid Electrolytes Extended Abstracts," Second International Meeting on Solid Electrolytes St. Andrews Ecosse.

- [11] Tarascon, J. M., and Armand, M., 2001, "Issues and Challenges Facing Rechargeable Lithium Batteries," *Nature*, 414(6861), pp. 359-367.
- [12] Vashishta, P., Mundy, J. N., and Shenoy, G. K., 1979, *Fast Ion Transport in Solids, Electrodes, and Electrolytes: Proceedings of The International Conference on Fast Ion Transport in Solids, Electrodes, and Electrolytes, Lake Geneva, Wisconsin, U.S.A., May 21-25, 1979, United States.*
- [13] Wright, P. V., 1975, "Electrical Conductivity in Ionic Complexes of Poly(Ethylene Oxide)," *British Polymer Journal* pp. 319-327.
- [14] Berthier, C., Gorecki, W., Minier, M., Armand, M. B., Chabagno, J. M., and Rigaud, P., 1983, "Microscopic Investigation of Ionic-Conductivity in Alkali-Metal Salts Poly(Ethylene Oxide) Adducts," *Solid State Ionics*, 11(1), Pp. 91-95.
- [15] Mullerplathe, F., and Vangunsteren, W. F., 1995, "Computer-Simulation of A Polymer Electrolyte - Lithium Iodide in Amorphous Poly(Ethylene Oxide)," *Journal of Chemical Physics*, 103(11), pp. 4745-4756.
- [16] Li, Q., Wood, E., and Ardebili, H., 2013, "Elucidating The Mechanisms of Ion Conductivity Enhancement in Polymer Nanocomposite Electrolytes for Lithium Ion Batteries," *Applied Physics Letters*, 102(24), Pp. 243903-243903-243905.
- [17] Yoshio, M., Brodd, R. J., and Kozawa, A., 2009, *Lithium-Ion Batteries*, Springer.
- [18] Gray, F. M., 1997, *Polymer Electrolytes*, England.
- [19] Croce, F., Appetecchi, G. B., Persi, L., and Scrosati, B., 1998, "Nanocomposite Polymer Electrolytes for Lithium Batteries," *Nature*, 394(6692), pp. 456-458.

- [20] Jung, S., Kim, D. W., Lee, S. D., Cheong, M., Nguyen, D. Q., Cho, B. W., and Kim, H. S., 2009, "Fillers for Solid-State Polymer Electrolytes: Highlight," *Bulletin of The Korean Chemical Society*, 30(10), pp. 2355-2361.
- [21] Scrosati, B., 1993, *Applications of Electroactive Polymers*, Chapman & Hall, New York.
- [22] McCarthy, D. W., Mark, J. E., Clarson, S. J., and Schaefer, D. W., 1998, "Synthesis, Structure, and Properties of Hybrid Organic-Inorganic Composites Based on Polysiloxanes. II. Comparisons Between Poly(Methylphenylsiloxane) and Poly(Dimethylsiloxane), and between Titania and Silica," *Journal of Polymer Science Part B-Polymer Physics*, 36(7), pp. 1191-1200.
- [23] Giannelis, E. P., 1996, "Polymer Layered Silicate Nanocomposites," *Advanced Materials*, 8(1), pp. 29.
- [24] Novak, B. M., 1993, "Hybrid Nanocomposite Materials - between Inorganic Glasses and Organic Polymers," *Advanced Materials*, 5(6), pp. 422-433.
- [25] Kumar, B., and Scanlon, L. G., 1994, "Polymer-Ceramic Composite Electrolytes," *Journal of Power Sources*, 52(2), pp. 261-268.
- [26] Dikin, D. A., Stankovich, S., Zimney, E. J., Piner, R. D., Dommett, G. H. B., Evmenenko, G., Nguyen, S. T., and Ruoff, R. S., 2007, "Preparation and Characterization of Graphene Oxide Paper," *Nature*, 448(7152), pp. 457-460.
- [27] Pandey, D., Reifengerger, R., and Piner, R., 2008, "Scanning Probe Microscopy Study of Exfoliated Oxidized Graphene Sheets," *Surface Science*, 602(9), pp. 1607-1613.

- [28] Mahmoud, W. E., 2011, "Morphology and Physical Properties of Poly(Ethylene Oxide) Loaded Graphene Nanocomposites Prepared by Two Different Techniques," *European Polymer Journal*, 47(8), pp. 1534-1540.
- [29] Tang, C., Hackenberg, K., Fu, Q., Ajayan, P. M., and Ardebili, H., 2012, "High Ion Conducting Polymer Nanocomposite Electrolytes Using Hybrid Nanofillers," *Nano Letters* 12(3), P. 1152.
- [30] Chen, Y. T., Chuang, Y. C., Su, J. H., Yu, H. C., and Chen-Yang, Y. W., 2011, "High Discharge Capacity Solid Composite Polymer Electrolyte Lithium Battery," *Journal of Power Sources*, 196(5), pp. 2802-2809.
- [31] Walls, H. J., Zhou, J., Yerian, J. A., Fedkiw, P. S., Khan, S. A., Stowe, M. K., And Baker, G. L., 2000, "Fumed Silica-Based Composite Polymer Electrolytes: Synthesis, Rheology, and Electrochemistry," *Journal of Power Sources*, 89(2), pp. 156-162.
- [32] Ji, K. S., Moon, H. S., Kim, J. W., and Park, J. W., 2003, "Role of Functional Nano-Sized Inorganic Fillers in Poly(Ethylene) Oxide-based Polymer Electrolytes," *Journal of Power Sources*, 117(1-2), pp. 124-130.
- [33] Hench, L. L., and West, J. K., 1990, *Principles of Electronic Ceramics*, United States.
- [34] Dreyer, D. R., Park, S., Bielawski, C. W., and Ruoff, R. S., 2010, "The Chemistry of Graphene Oxide," *Chemical Society Reviews*, 39(1), pp. 228-240.
- [35] Mobasherpour, I., Salahi, E., and Ebrahimi, M., 2012, "Removal of Divalent Nickel Cations From Aqueous Solution by Multi-Walled Carbon Nano Tubes: Equilibrium and Kinetic Processes," *Research on Chemical Intermediates*, 38(9), pp. 2205-2222.

- [36] Yang, S.-T., Chang, Y., Wang, H., Liu, G., Chen, S., Wang, Y., Liu, Y., and Cao, A., 2010, "Folding/Aggregation of Graphene Oxide and Its Application in  $\text{Cu}_2^+$  Removal," *Journal of Colloid and Interface Science*, 351(1), pp. 122-127.
- [37] Nan, C. W., Fan, L. Z., Lin, Y. H., and Cai, Q., 2003, "Enhanced Ionic Conductivity of Polymer Electrolytes Containing Nanocomposite  $\text{SiO}_2$  Particles," *Physical Review Letters*, 91(26).
- [38] Money, B. K., Hariharan, K., and Swenson, J., 2012, "Glass Transition and Relaxation Processes of Nanocomposite Polymer Electrolytes," *Journal of Physical Chemistry B*, 116(26), pp. 7762-7770.
- [39] Ratna, D., Divekar, S., Patchaiappan, S., Samui, A. B., and Chakraborty, B. C., 2007, "Poly(Ethylene Oxide)/Clay Nanocomposites for Solid Polymer Electrolyte Applications," *Polymer International*, 56(7), pp. 900-904.
- [40] Appetecchi, G. B., Croce, F., Persi, L., Ronci, F., and Scrosati, B., 2000, "Transport and Interfacial Properties of Composite Polymer Electrolytes," *Electrochimica Acta*, 45(8), pp. 1481-1490.
- [41] Pengju, P., Li, Z., Jinjun, Y., and Yoshio, I., 2013, "Fractional Crystallization and Phase Segregation in Binary Miscible Poly(Butylene Succinate)/Poly(Ethylene Oxide) Crystalline Blends: Effect of Crystallization Temperature," *Macromolecular Materials and Engineering*, 298(2), P. 201.
- [42] Li, Z. H., Zhang, H. P., Zhang, P., Li, G. C., Wu, Y. P., and Zhou, X. D., 2008, "Effects of The Porous Structure on Conductivity of Nanocomposite Polymer Electrolyte for Lithium Ion Batteries," *Journal of Membrane Science*, 322(2), pp. 416-422.

- [43] Bonet, F., Guery, C., Guyomard, D., Urbina, R. H., Tekaiia-Elhsissen, K., and Tarascon, J. M., 1999, "Electrochemical Reduction of Noble Metal Species in Ethylene Glycol at Platinum and Glassy Carbon Rotating Disk Electrodes," *Solid State Ionics*, 126(3-4), pp. 337-348.
- [44] Xi, J. Y., Qiu, X. P., Ma, X. M., Cui, M. Z., Yang, J., Tang, X. Z., Zhu, W. T., and Chen, L. Q., 2005, "Composite Polymer Electrolyte Doped with Mesoporous Silica SBA-15 for Lithium Polymer Battery," *Solid State Ionics*, 176(13-14), pp. 1249-1260.
- [45] Pandey, K., Dwivedi, M. M., Tripathi, M., Singh, M., and Agrawal, S. L., 2008, "Structural, Thermal and Ion Transport Studies on Nanocomposite Polymer Electrolyte- $\{(PEO + SiO_2):NH_4 SCN\}$  System," *Ionics*, 14(6), pp. 515-523.
- [46] Barroso-Bujans, F., Fernandez-Alonso, F., Pomposo, J. A., Enciso, E., Fierro, J. L. G., and Colmenero, J., 2012, "Tunable Uptake of Poly(Ethylene Oxide) by Graphite-Oxide-based Materials," *Carbon*, 50(14), pp. 5232-5241.
- [47] Barroso-Bujans, F., Cervený, S., Alegría, A., and Colmenero, J., 2010, "Sorption and Desorption Behavior of Water and Organic Solvents from Graphite Oxide," *Carbon*, 48(11), pp. 3277-3286.
- [48] Cervený, S., Barroso-Bujans, F., Alegria, A., and Colmenero, J., 2010, "Dynamics of Water Intercalated in Graphite Oxide," *Journal of Physical Chemistry C*, 114(6), pp. 2604-2612.